Molecular Therapy

Original Article



A single dose of a vectorized mAb targeting TDP-43 potently inhibits the neuropathology in a model of ALS/FTD

Greg del Val,¹ Florence Gauye,¹ Mickaël Audrain,¹ Sébastien Menant,¹ Monisha Ratnam,¹ Elodie Chevalier,¹ Romain Ollier,¹ Daisy Bhatia,¹ Tamara Seredenina,¹ Tariq Afroz,¹ Andrea Pfeifer,¹ Marie Kosco-Vilbois,¹ and Damien Nevoltris¹

¹AC Immune SA, 1015 Lausanne, Switzerland

Transactive response DNA binding protein-43 (TDP-43)mediated pathology is a hallmark of devastating neurodegenerative diseases, including amyotrophic lateral sclerosis (ALS) and frontotemporal dementia (FTD). Thus, monoclonal antibodies (mAbs) are being developed to target the pathological forms of this protein. To improve mAb exposure within the central nervous system, a potent anti-TDP-43 mAb, ACI-5891, was generated as a vectorized full-length antibody (vmAb) and evaluated for brain delivery using adeno-associated virus 9 (AAV9). Among the expression cassettes explored, the selected construct utilized an internal ribosome entry site (IRES), which produced high expression yields in vitro (>200 mg/L) with comparable quality, binding, and functional properties to the conventionally produced mAb. A single intracisternal administration of vmAb ACI-5891 demonstrated a broad brain distribution and sustained expression (i.e., months) in the serum, cerebrospinal fluid, and brain of mice. In a mouse model of ALS/FTD, treatment with a vmAb reduced the amount of pathological phospho-TDP-43 in neurons by 58% and 68% when expressed using either a ubiquitous promoter or a brain-selective promoter, respectively. This innovative approach sufficiently delivers effective immunotherapy with a single dose and illustrates the enormous potential of using vectorized antibodies to target neuropathology, including TDP-43 in patients suffering from ALS, FTD, and other TDP-43 proteinopathies.

INTRODUCTION

Transactive response DNA binding protein-43 (TDP-43) plays an important homeostatic role in RNA processing and gene regulation within the cell nucleus and cytoplasm.¹ Abnormal accumulation of ubiquitinated and phosphorylated TDP-43 in the cytoplasm of neurons and glial cells was identified as a pathological hallmark of amyotrophic lateral sclerosis (ALS), frontotemporal dementia (FTD), and LATE (limbic-predominant age-related TDP-43 encephalopathy).^{2–5} TDP-43-associated pathology occurs in 97% of ALS cases and approximately half of FTD cases, driving the growing interest to use TDP-43 as a drug target.^{6,7} Moreover, path-

ological TDP-43 has been observed in neurodegenerative diseases such as Alzheimer's (AD), Parkinson's (PD) and Huntington's disease (HD).^{8,9} Extracellular prion-like spreading may occur with pathological TDP-43 in a seed-dependent and self-templating manner. 10 It involves the release of TDP-43 aggregates from affected neurons, uptake by neighboring cells, and the subsequent propagation of pathology across different brain regions. 11 To date, the available treatments for ALS are limited to managing symptoms.¹² Disease-modifying drugs, such as tofersen, are an important step forward but only indicated for patients with superoxide dismutase 1 (SOD1) mutations, a small subset of all ALS cases.¹³ Thus, immunotherapies targeting extracellular TDP-43 are a viable therapeutic approach to offer clinical benefits to patients suffering from TDP-43 proteinopathies including ALS and frontotemporal lobar degeneration with TDP-43-immunoreactive pathology (FTLD-TDP).

We recently demonstrated that targeting pathological TDP-43, by administering the monoclonal antibody (mAb) ACI-5891, weekly over 3 months, resulted in significant inhibition of neuropathology, conferring neuroprotection in two different mouse models of ALS/FTD.¹⁴ While successful, to obtain effective drug exposure in the brain to neutralize the extracellular target within the CNS required both frequent injections and high doses of the mAb ACI-5891. Building on this proof of mechanism data, achieving the same or better exposure and efficacy with a single-dose administration would significantly improve the clinical management and quality of life with such diseases. Thus, we set out to develop a delivery system to administer a full-length antibody format in conjunction with adeno-associated virus (AAV) vector.

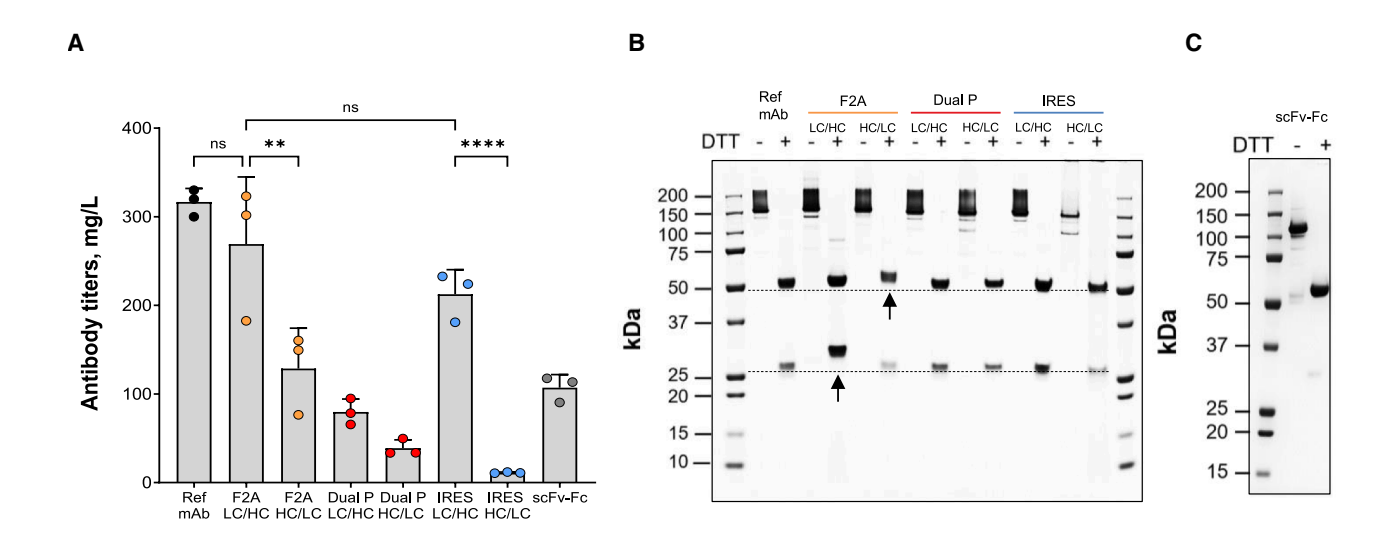
For this, a significant challenge is to vectorize a full-length antibody gene (i.e., vmAb), within an AAV expression cassette that is limited

Received 18 November 2024; accepted 11 June 2025; https://doi.org/10.1016/j.ymthe.2025.06.026.

Correspondence: Damien Nevoltris, AC Immune SA, EPFL Innovation Park, Building B, 1015 Lausanne, Switzerland.

E-mail: damien.nevoltris@acimmune.com





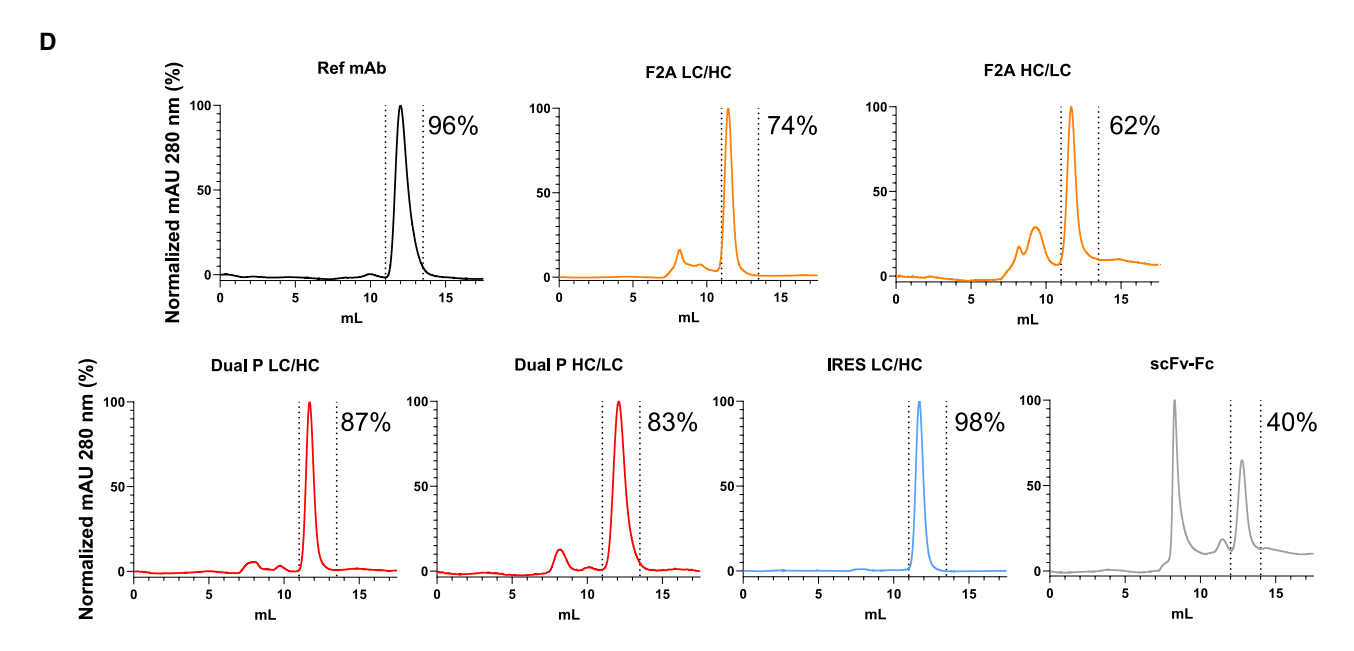


Figure 1. Characteristics of mAbs and scFv-Fc produced in mammalian cells

(A) Expression titer of ACI-5891 mAbs and scFv-Fc in CHO cell supernatant 12 days following transfection. Antibody quantification is performed by bio-layer interferometry (BLI) with protein A-coated biosensors. Antibody expression is driven by the cytomegalovirus (CMV) promoter. In the case of constructions with two promoters, the light chain (LC) is controlled by CMV and heavy chain (HC) by SV40 promoter. Construction designs are illustrated in Figure S1. Ref mAb represents the anti-TDP-43 mouse IgG2a ACI-5891 produced conventionally using two independent plasmids. Other conditions refer to mAb ACI-5891 produced using a ubiquitous expression cassette using furin/2A self-cleaving peptide (F2A), two promoters (Dual P), or an internal ribosome entry site (IRES). ScFv-Fc refers to the variable fragments of ACI-5891 fused to mouse IgG2a Fc domain. Data are shown as mean (SD); ordinary one-way ANOVA followed by a Tukey's test for multiple comparisons, reported as ** $p \le 0.0024$ and ****p < 0.0001. (B) SDS-PAGE 4%–12% separation of 1 μ g purified antibodies under non-reducing or reducing conditions (5 mM dithiothreitol, DTT) followed by Coomassie blue staining. Dotted lines highlight the expected molecular weight for LC (~25 kDa) and HC (~50 kDa) using Ref mAb as standard. (C) SDS-PAGE separation of anti-TDP-43 scFv-Fc under same conditions. (D) Size exclusion chromatography analysis of purified full-length IgG and scFv-Fc using Superdex 200 Increase 10/300GL column. Separations were performed in PBS buffer at 4°C. The fraction of monomeric protein was calculated as the ratio of the monomer peak area to the total area of the chromatogram, as measured by UV absorbance at 280 nm.

to 4,700 bp as a single-strand DNA (ssDNA) while still maintaining the quality of the expressed antibody.¹⁵ To address this need, the antibody genes were incorporated into various mono- and bicis-

tronic expression cassettes. Next, the orientation of the light versus heavy chains (HCs) in the vector was also explored in order to reach comparable expression levels to the gold standard cassette design (i.

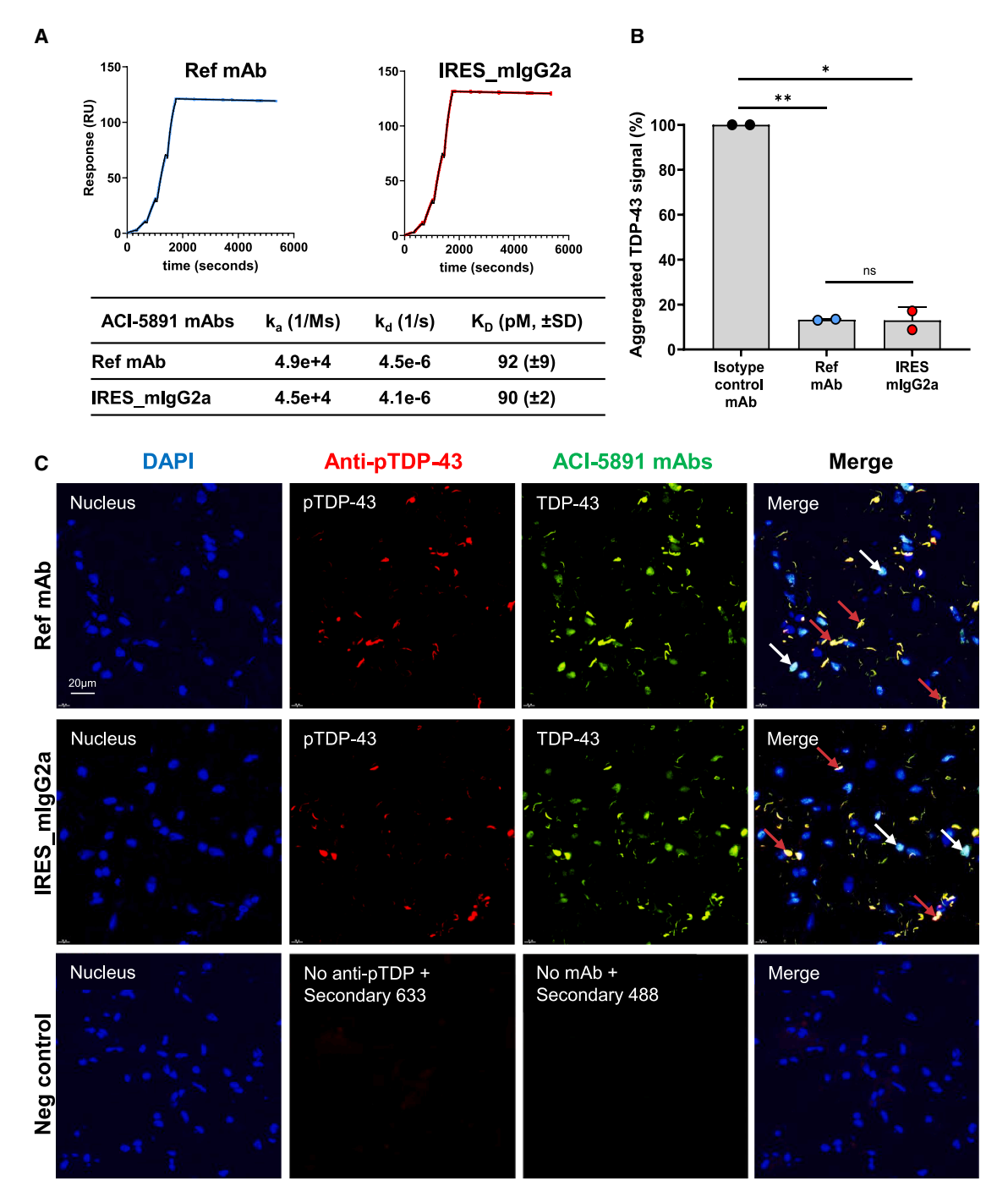


Figure 2. Characterization of binding properties and aggregation inhibition of ACI-5891 mAbs

(A) Surface plasmon resonance (SPR) analysis of reference mAb ACI-5891 (mouse $\lg G2a$) produced using conventional two-plasmid expression (blue sensorgram, left panel) compared to the IRES-linked light and heavy chain (LC/HC) ACI-5891 produced using a bicistronic construct (red sensorgram, right panel). Binding affinities are measured against the immobilized full-length soluble human TDP-43. The lower panel table compiles mean kinetic constants derived from sensorgrams fitted with 1:1 Langmuir model (black curves, n=2). (B) TDP-43 de novo aggregation upon cleavage of MBP tag by specific tobacco etch virus (TEV) was analyzed in the presence of isotype control mAb, Ref mAb ACI-5891, or IRES_ $\lg G2a$ mAb. The inhibition of aggregation was measured by absorbance (OD600nm, y axis) at 24 h post-MBP cleavage, at room temperature. The mouse-derived sequence of trastuzumab was used as isotype control. Data are shown as mean (SD) of two independent experiments (n=2), performed in technical triplicates. Unpaired t tests with a Welch's correction for the comparison with isotype control reported as ** $p \le 0.01$, * $p \le 0.05$. (C) Immunostaining of pathological postmortem human brain from FTLD-TDP type A case. The three rows represent staining with the reference anti-TDP-43 mAb mlgG2a ACI-5891 (Ref mAb, top row), the

(legend continued on next page)

e., 2A self-cleavage peptides). ^{16–18} Together, the optimal internal ribosome entry site (IRES) approach was identified, providing vmAbs with comparable quality, binding, and functional properties to the original parental mAb produced by classical methodology and superiority over 2A-based designs.

In vivo, a single intracisternal injection of the vectorized full-length antibody produced sustained vmAb expression in the serum, cerebrospinal fluid (CSF), and brain of mice for over 4 months. Furthermore, this single administration resulted in the significant reduction of pathological TDP-43 in a mouse model of ALS/FTD as reported for the parental mAb. ¹⁴ Thus, the present report is the first to show efficacy of a vectorized full-length antibody targeting TDP-43 that inhibits the neuropathology in a model of human neurodegenerative disease. Such innovative approaches are desperately needed to address these devastating diseases that impose a high burden of emotional and financial costs on families and society.

RESULTS

Generation of a high-quality anti-TDP-43 full-length antibody using bicistronic plasmids

The selection criteria chosen to identify the best expression cassette design for AAV delivery was based on antibody quality attributes including protein titers, propensity to aggregate, monomeric content, and binding affinity to target protein. The benchmark anti-human TDP-43 mAb, ACI-5891 (Ref mAb), a mouse IgG2a, was conventionally produced in Chinese hamster ovary (CHO) cells, using 2 different plasmids, one expressing the light chain (LC) and the second expressing the heavy chain (HC) (Figure S1A). Using the same ACI-5891 sequence, a panel of bicistronic cassettes were generated involving a furin/2A self-cleavage peptide (F2A), two promoters (Dual P), or an IRES sequence. Two versions of each bicistronic expression cassette were created by inverting the HC and LC (Figure S1B). A monocistronic gene coding for a scFv-Fc (single-chain variable fragment fused to Fc domain) variant of ACI-5891 was produced as an additional control for expression and quality (Figure S1C). These expression cassettes were generated using a plasmid suitable for AAV production, and the corresponding antibodies were produced in a CHO mammalian cell line using transient transfection.

Antibody titers were quantified in the supernatant of CHO cells 12 days after transfection (Figure 1A). The expression of the conventionally produced anti-TDP-43 reference mAb ACI-5891 yielded 316 mg/L. For a particular bicistronic construct pair, positioning the LC gene before the HC consistently resulted in higher antibody expression. F2A and IRES (LC/HC) designs produced similar antibody levels, while the dual promoter strategies and monocistronic scFv-Fc construct yielded lower antibody levels (<100 mg/L). The most signif-

icant difference within a pair was observed in the IRES-containing cassettes, with IRES-LC/HC yielding more than 200 mg/L, compared to 10 mg/L for IRES-HC/LC, representing a 20-fold increase in antibody production. Since the HC of an antibody cannot be folded and exported without the LC, these results are expected when using an IRES sequence, as the downstream gene is expressed at lower levels (i.e., 30%–50%) compared to the upstream gene. ^{19,20}

Next, molecular weights (MWs) of the purified anti-TDP-43 ACI-5891 mAbs (Figure 1B) and scFv-Fc version (Figure 1C) were analyzed by SDS-PAGE. Non-reducing conditions confirmed formation of interchain disulfide bonds for all mAbs, while reducing conditions demonstrated a difference between the expression cassettes evaluated. The dual promoters and IRES-based constructs displayed expected MWs for the HC and LC, similar to the reference mAb. However, the F2A approach generated mAbs with shifted MW profiles for both the HCs and LCs (black arrows, Figure 1B). This result suggests suboptimal proteolytic cleavage during antibody secretion, leading to the retention of additional amino acids upstream of the cleavage site. Indeed, remaining amino acids from furin/2A sequences were observed by liquid chromatography with tandem mass spectrometry (LC-MS/MS) using a control mAb (Figure S2; Table S1).

To monitor antibody degradation and aggregate levels, size exclusion chromatography (SEC) was used. As shown in Figure 1D, the reference mAb was well folded, with a 96% monomeric immunoglobulin G (IgG) content eluting at 12 mL under these conditions, as expected. In contrast, antibodies produced using the F2A cassette had substantial aggregate levels, with monomeric IgG representing \sim 74% for the F2A-LC/HC construct and \sim 62% for F2A-HC/LC. Interestingly, the monomeric peak of the furin/2A cassette, expected between 11 and 13.5 mL, displayed a lower retention time compared the reference and other mAbs, correlating with the SDS-PAGE and LC-MS/MS data. Antibody produced with the dual promoters had a lower aggregate level compared to F2A constructs but yielded a lower quality than the Ref mAb, with a monomeric content below the 95% purity cutoff. Antibody produced using the IRES-LC/HC expression cassette displayed a high-quality profile with 98% monomeric mAb and no aggregation. The known poor stability of scFv-Fc constructs was confirmed,²¹ with only 40% monomeric species and considerable levels of aggregates. Due to the low antibody titers obtained using the IRES-HC/LC construct, the purified quantity was not sufficient to be analyzed by SEC. To confirm the robustness of the IRES strategy, the sequence of a marketed mAb, trastuzumab, was also produced using the IRES approach and provided comparable results, achieving 97% of monomeric IgG (Figure S3). Taken together, antibodies produced by the IRES-LC/HC bicistronic

ACI-5891 mAb produced with IRES-mlgG2a expression cassette (middle row), and no primary mAbs (Neg control, bottom row). DAPI is used to localize cell nuclei (blue), and phosphorylated TDP-43 (i.e., pathological TDP-43) is detected by anti-pS409/410 antibody + secondary A633 (Red). ACI-5891 mAbs bind to TDP-43 and are detected using secondary anti-mouse A488 (green, third column). The merge column (far right) combines all signals. Physiological and pathological forms of TDP-43 labeled with ACI-5891 mAbs are indicated with white and red arrows, respectively. White scale bar on bottom left of images represents 20 µm.

cassette demonstrated the best expression and quality and were therefore further characterized.

ACI-5891 produced by the IRES expression cassette retains binding and functional properties

Having selected the IRES-LC/HC cassette, both the mouse IgG2a (IRES_mIgG2a) and a human IgG1 chimeric (IRES_hIgG1) version of ACI-5891 mAb were generated. Since mouse IgG2a is structurally and functionally the closest equivalent to human IgG1 and is immunotolerant, it is the preferred subclass for preclinical mouse models when effector function is required. Conversely, human IgG1 is particularly advantageous for easier detection in mice, during short-time exposures (2–4 weeks). Both antibody versions were characterized *in vitro* before *in vivo* studies. Using surface plasmon resonance (SPR), binding kinetics of the IRES_mIgG2a for soluble recombinant human TDP-43 demonstrated a K_D comparable to the Ref mAb with measured affinities of 90 and 92 pM, respectively (Figure 2A). Similar results were obtained for the chimeric Ref mAb-hIgG1 and the antibody produced with IRES_hIgG1 expression cassette, with a comparable K_D of 87 and 92 pM, respectively (Figure S4A).

Then, to assess the inhibition of TDP-43 aggregation by the ACI-5891 mAb, *de novo* aggregates of human TDP-43 were induced in the presence of the antibody. An isotype control mAb (i.e., not interfering with aggregation) was used to establish the baseline, representing 100% aggregation level (Figure 2B). The Ref mAb and IRES_mIgG2a demonstrated strong inhibition of TDP-43 aggregation, by reducing the formation of *de novo* aggregates by 87% for both versions of ACI-5891 (Figure 2B). The full aggregation kinetics did not show any differences between the Ref mAb, the IRES_mIgG2a, and the no-aggregation control condition (i.e., without tobacco etch virus [TEV] protease cleavage, Figures S5A and S5B).

Finally, target engagement of IRES_mIgG2a was analyzed by immunofluorescence (IF) on brain sections prepared postmortem from patients with FTLD-TDP. For localization of nuclei and to identify phosphorylated TDP-43 (pTDP-43) inclusions, sections were labeled with DAPI and an anti-phospho-TDP-43 mAb (anti-pTDP-43 S409/ 410), respectively (Figure 2C). To establish the level of background, panels are included representing incubation with the secondary antibody alone (i.e., Neg control; Figure 2C). Incubation with the Ref mAb ACI-5891 and IRES_mIgG2a provides comparable labeling of both pathological (red arrows) and physiological (white arrows) forms of TDP-43, as expected. 14 Similar labeling pattern were obtained using the chimeric human IRES_hIgG1 construction (Figure S4B). Taken together, the anti-TDP-43 ACI-5891 mAb, produced using the bicistronic IRES-LC/HC expression cassette, provided binding and functional properties comparable to the original, conventionally produced recombinant mAb.

Promoters regulate expression of the vectorized ACI-5891 antibody, post-transduction of rat primary cortical cultures

Given the desired quality of the antibody produced using the IRES-LC/HC expression cassette, the construct was selected to generate

single-stranded DNA adeno-associated viruses (ssDNA AAVs), for *in vitro* and *in vivo* delivery. The vectorized version of ACI-5891 (i.e., mAb genes in AAV9) was used to transduce CHO cells, and the expressed antibody (vmAb) was subsequently purified to assess quality. The profile obtained for the vmAb (produced using AAV) was identical to the mAb produced only using the plasmid (used in Figures 1 and 2), exhibiting expected MWs and a high monomeric content (>98%; Figure S6).

Next, to assess the expression titer and binding capability (i.e., target engagement) of the secreted vmAbs under more physiological conditions, primary cortical cultures from rat brains were transduced with AAV2 and AAV9 encoding the hIgG1 ACI-5891, driven by the ubiquitous CMV (cytomegalovirus) promoter (Figure 3A). The choice of these two serotypes was considered based on their safe and broad clinical application, providing natural transduction capabilities to brain endothelial cells or cells from CNS, respectively. The vmAbs were quantified in primary cells supernatant 7 days post-transduction, using an antigen ELISA (TDP-43-coated plates) to assess retained target affinity. The primary cells transduced with AAV9 produced significantly higher vmAbs titers (400 $\mu g/L$) compared to AAV2 (4 $\mu g/L$, Figure 3A). Hence, AAV9 was chosen for further development.

As neurons and motor neurons are impaired in patients with ALS or FTD, our strategy aims to deliver the mAb transgene predominantly in glial cells, which may be suitable to high secretion level,²⁸ and will serve as in vivo antibody factory in the brain. Previous studies have shown that AAV containing the CMV promoter produced strong expression in glial cells as compared to neurons.^{29,30} To provide options as to which cell type to be transduced in vivo, and potentially achieving selectivity of production, two ubiquitous promoters, CMV and CBh,³¹ and two glial cell selective promoters, OLIG2 and GFAP, 32,33 were evaluated using AAV9 vector. To enhance vmAb expression, the CMV enhancer (CMVe) was subcloned upstream of the OLIG2 and GFAP promoters, creating eOLIG2 and eGFAP promoters, respectively. Both the mouse IgG2a (AAV9_mIgG2a) and human IgG1 chimeric (AAV9_hIgG1) versions of the anti-TDP-43 ACI-5891 vmAb were evaluated for expression. Similar results were observed for either the mouse or human vmAbs (Figures 3B and 3C, respectively). The CMV promoter yielded the lowest vmAb titer, with 70 μg/L after 7 days for the two vmAb versions. The eOLIG2 and eGFAP promoters improved the vmAb titer by 3-fold compared to the CMV promoter while the CBh promoter provided a 6-fold improvement, resulting in a yield over 400 μg/L vmAb from the primary cell co-culture.

To determine which cell type from the co-culture was producing the vmAb, immunolabeling was performed using an anti-mouse IgG2a antibody (to detect the mIgG2a ACI-5891 vmAb), anti-MAP2 for neurons, and anti-GFAP for astrocytes (Figure 3D). The CBh promoter appeared to produce the strongest signal when comparing the intensity of the anti-mouse IgG2a labeling, similar to the titers quantified in the supernatant of the co-cultures, described in

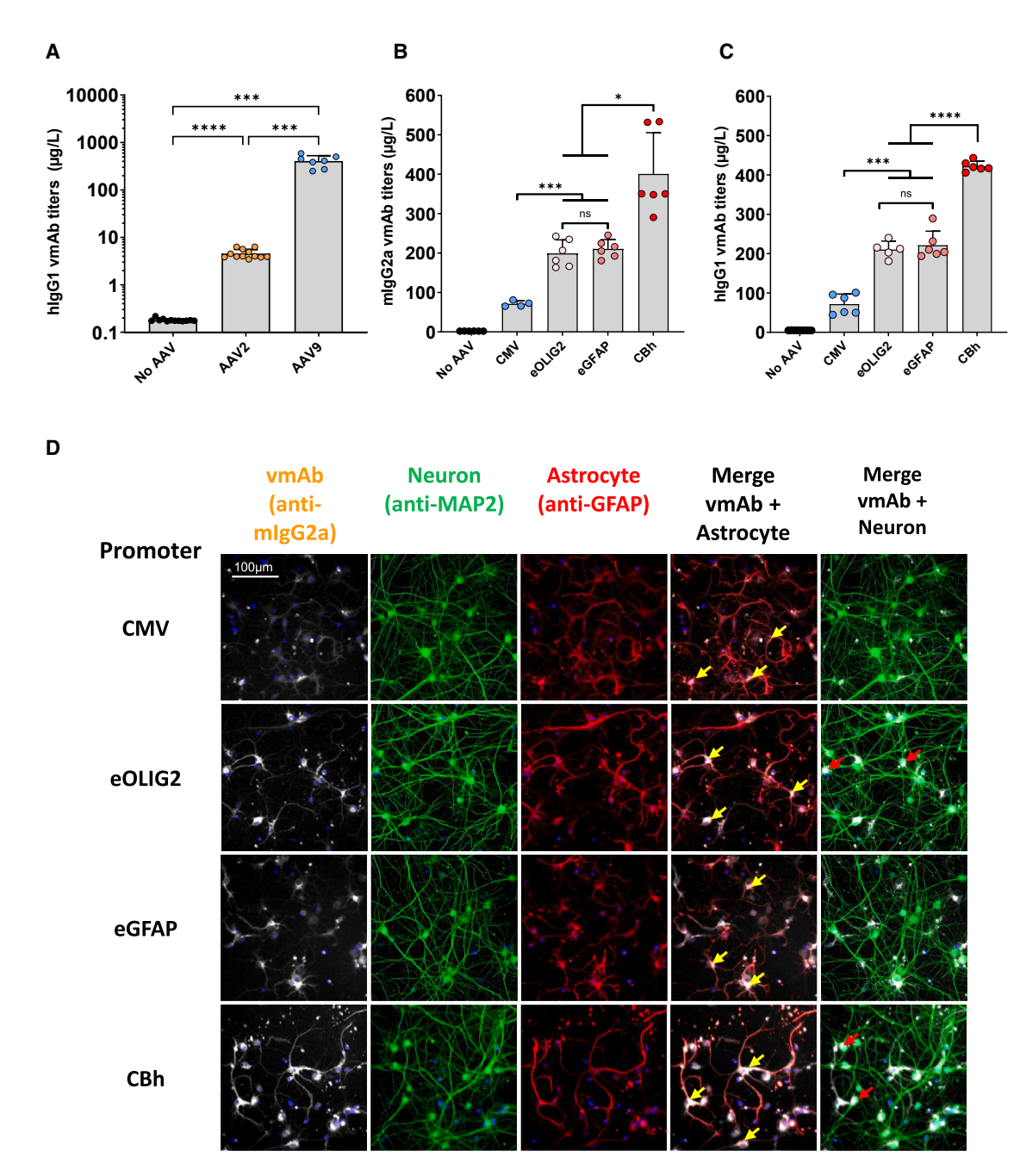


Figure 3. Characterization of vectorized ACI-5891 expression in rat primary cortical cultures

(A) Human IgG1 vmAb titers quantified in supernatant of rat primary cortical cultures (40K cells/well), 7 days post-AAV transduction with 100K as multiplicity of infection (MOI). Expression of vmAb is driven by CMV promoter for either AAV2 or AAV9. The vmAbs are quantified in cell supernatant using a TDP-43 ELISA. Data are shown as mean (SD); ordinary one-way ANOVA followed by a Dunnett's T3 test for multiple comparisons as *** $p \le 0.003$ and ****p < 0.0001. (B) Mouse IgG2a and (C) human ACI-5891 IgG1 vmAb titers quantified in supernatant of rat primary cortical cultures (40K cells/well) using a human TDP-43 ELISA after 7 days post-transduction using AAV9 (MOI: 100K). Expression of vmAb is driven by different promoters, such as CMV, eOLIG2, eGFAP, and CBh. Data are shown as mean (SD); ordinary one-way ANOVA followed by a Dunnett's T3 test for multiple comparisons, reported as * $p \le 0.0486$, *** $p \le 0.0009$, and ****p < 0.0001. (D) Immunolabeled rat brain primary cells expressing mlgG2a vmAb after transduction with AAV9 using CMV, eOLIG2, eGFAP and CBh promoters. Cells were labeled with the following antibodies: anti-mouse IgG2a (white), to detect ACI-5891 vmAb expression; anti-MAP2 (green), to identify neuronal cells; and anti-GFAP (red), to identify astrocytes. The co-localization of the white signal with red indicates vmAb expression by astrocytes (yellow arrowhead). Co-localization of the white signal with green indicates vmAb expression by neurons (red arrowhead). To visualize cell nuclei, cells were stained with DAPI dye (blue). Scale bar, 100 μ m.

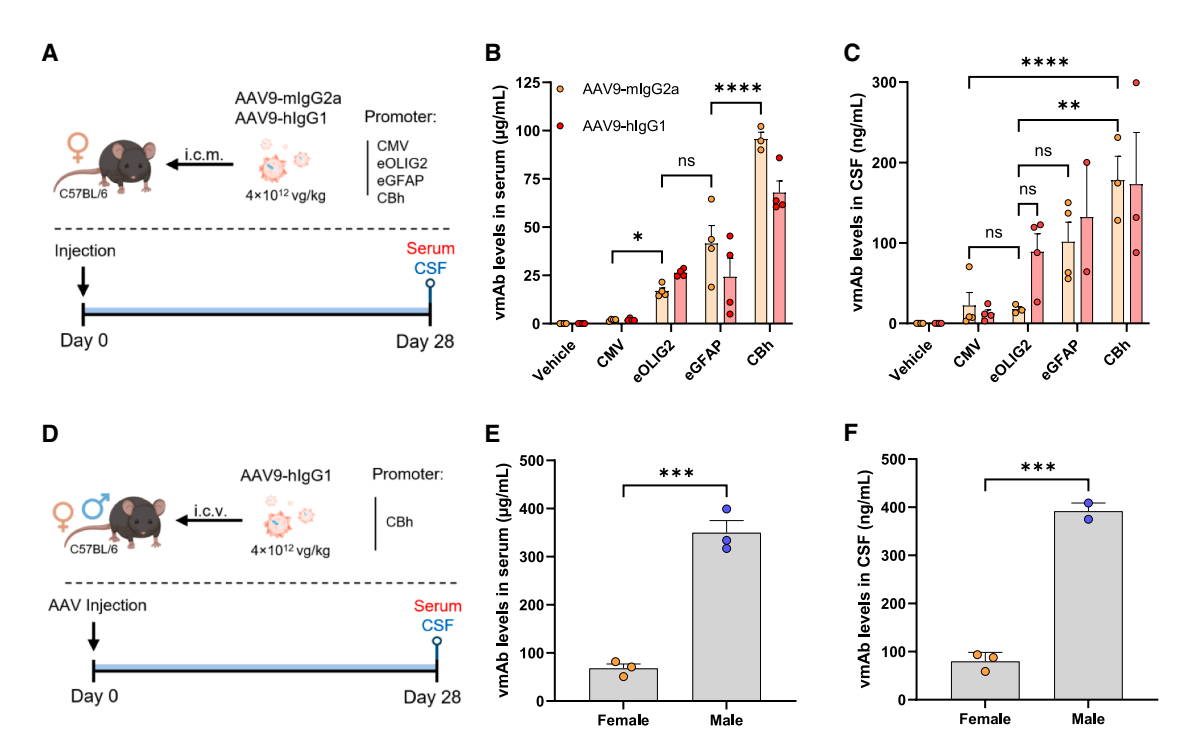


Figure 4. AAV9-mediated vmAb expression in vivo

(A) Schematic representation of the *in vivo* study design. Female C57BL/6 WT mice were intracisternally (i.c.m.) administered a single dose of 4×10^{12} vg/kg (i.e., $\sim 1 \times 10^{11}$ vg) AAV9-mlgG2a or AAV9-hlgG1, encoding the mouse or human ACI-5891 lgG, respectively (vmAbs). Each AAV was generated using the CMV, eOLIG2, eGFAP, or CBh promoter. Intracisternal injection was performed at day 0. Serum and CSF were collected at terminal time point (28 days). (B) vmAb levels in serum and (C) in CSF of C57BL/6 WT female mice, at 28 days post-single dose administration of AAV9-mlgG2a (orange) or AAV9-hlgG1 (red). vmAbs were measured using a TDP-43-based ELISA to assess retained target engagement (μ g/mL for serum and ng/mL for CSF, y axis). Data are shown as mean (SD); ordinary two-way ANOVA followed by a Tukey's test for multiple comparisons, reported as * $p \le 0.484$, ** $p \le 0.033$, and ****p < 0.0001. (D) Schematic representation of the *in vivo* study design. Male and female C57BL/6 WT mice received a single intracerebroventricular (i.c.v.) dose of 4×10^{12} vg/kg (i.e., $\sim 1 \times 10^{11}$ vg) AAV9-hlgG1, encoding the human ACI-5891 vmAb. AAV9-hlgG1 was generated using the CBh promoter. AAV administration was performed at day 0. Serum and CSF were collected at terminal time point (28 days). (E) vmAb levels in serum and (F) in CSF of male and female C57BL/6 WT mice. VmAbs levels are displayed in orange and blue circles for female and male, respectively. VmAbs were measured using a TDP-43-based ELISA (μ g/mL for serum and ng/mL for CSF, y axis). Data are shown as mean (SD); unpaired t test was used for statistical analysis and reported as *** $p \le 0.0005$.

Figures 3B or 3C. As expected, the CMV, CBh, and eGFAP promoters resulted in robust vmAb expression by astrocytes (Figure 3D, merge panel, yellow arrowheads). Surprisingly, the eO-LIG2 promoter similarly resulted in robust astrocytic-selective vmAb expression (merge, yellow arrowheads) but, similar to the CBh promoter, did induce some expression in neurons as well (merge, red arrowheads).

In summary, a controlled and astrocyte-targeted expression of mouse and human AAV9-delivered ACI-5891 vmAb was achieved. The ubiquitous CBh and astrocyte-selective eGFAP promoters provided the highest vmAb expression by glial cells *in vitro*.

AAV9-mediated vmAb expression drives sustained functional antibody titers in serum, CSF, and brain of mice

To evaluate *in vivo* expression of the vmAb, female C57BL/6 mice were intracisternally (i.c.m.) administered a single dose of 4×10^{12} vg/kg ($\sim 1 \times 10^{11}$ vg) AAV9-mIgG2a or AAV9-hIgG1, encoding the mouse or human anti-TDP-43 ACI-5891 antibody, respectively

(Figure 4A). To investigate comparability with the *in vitro* results, each version was generated using the CMV, eOLIG2, eGFAP, or CBh promoter. VmAb expression was evaluated in serum and CSF at 28 days post-administration, using a TDP-43-based ELISA. In serum, comparable vmAb titers were observed for the mouse and human versions for a given promoter (Figure 4B). The CMV promoter yielded the lowest titers, with less than 5 μ g/mL vmAbs detected at 28 days in serum. The eOLIG2 promoter yielded 17 and 26 μ g/mL, and the eGFAP promoter yielded 41 and 24 μ g/mL for the mouse and human vmAb version, respectively. Similar to the results observed using rat primary cortical cultures, the CBh promoter produced significantly higher vmAb titers compared to other promoters, achieving 95 μ g/mL (mIgG2a) and 68 μ g/mL (hIgG1) in serum.

In CSF (Figure 4C), a similar ranking was observed. Both the eGFAP and CBh promoters yielded a high vmAb expression reaching over 100 ng/mL, 28 days following a single intracisternal AAV administration. The difference for the eOLIG2 promoter for the mouse

IgG (16 ng/mL) versus the human IgG (90 ng/mL) was not significant and thus considered within the variability of the method. As similar high expression titers were obtained *in vitro* and *in vivo*, the CBh promoter was selected for further investigation.

To evaluate the influence of sex on vmAb expression, $^{34-37}$ a small study was conducted. A single intracerebroventricular (i.c.v.) dose of AAV9-hIgG1 (4 × 10¹² vg/kg) was administered to both male and female mice (Figure 4D). Similar to the data obtained using intracisternal AAV delivery (Figures 4B and 4C), the hIgG1 vmAb titers in females reached 68 µg/mL in serum and 80 ng/mL in CSF (Figures 4E and 4F). Strikingly, the vmAb titers in males were five times higher compared to females, with 350 µg/mL in serum and 392 ng/mL in CSF. Consistent with previous findings, 35 AAV9-mediated liver transduction and transgene expression were significantly higher in male mice than in females. A 12-fold increase in delivered DNA and a 7-fold higher mRNA level of vmAb ACI-5891 were measured in male liver samples compared to females (Figure S7). These data informed the design of the next studies to include and potentially keep separated the data for the two sexes.

To further evaluate antibody exposure levels and kinetics, a study was carried out comparing AAV9-mediated vmAb expression versus a standard passive immunotherapy approach. The mAb-hIgG1 was administered systemically to model a clinically relevant delivery approach for CNS-targeting therapies, while AAV was delivered within the CSF to improved CNS exposure, as systemic AAV9 administration often results in limited brain penetration. ACI-5891 hIgG1 levels were measured at different time points after either a single intraperitoneal (i.p.) bolus injection of the Ref mAb (60 mg/kg) or a single intra-CSF (i.c.m. or i.c.v.) administration of AAV9-CBh-hIgG1 at 4×10^{12} vg/kg producing the vmAb (Figure 5A). mAbs and vmAbs in serum and CSF were quantified using an anti-TDP-43 ELISA, ensuring effective target engagement. Additionally, the binding properties of the in vivo-produced vmAb ACI-5891 were compared to CHO-expressed Ref mAb. Indeed, the in vivo-produced vmAb demonstrated same affinity to hTDP-43 (human TDP-43) as compared to the recombinantly produced mAb (Figure S8). Following the i.p. bolus injection, the mAb reached a Cmax of 431 μg/mL in serum at 24 h (Figure 5B). As expected, mAb levels in serum cleared over time, reaching 5 µg/mL at day 28. In contrast, AAV9-mediated ACI-5891 vmAb exhibited an increasing (0-12 days) and sustained (12-28 days) expression over the 28-day period, with up to 350 µg/mL vmAb measured at the terminal time point for males. VmAb titers were significantly higher in males than in females, but no significant difference was observed between the intracisternal and i.c.v. route of administration evaluated, with both averaging 80 µg/mL vmAb at 28 days in female. To ensure accurate comparison between the different pharmacokinetic profiles of the two approaches (mAb vs. AAV-delivered vmAb), total serum exposure was measured as the area under the curve (AUC) over the 28 days period. The high dose of Ref mAb (60 mg/kg) reached an AUC of 1,281 μg·mL⁻¹·day, whereas the AAV approach achieved 6,395 μg·mL⁻¹·day vmAbs in males. (Table 1). AAV9-mediated vmAb resulted in up to 5-fold higher serum exposure compared to the high-dose passive immunotherapy approach. In females, comparable exposure levels were observed for AAV approach vs. bolus mAb administration, regardless of the administration route (i.c.m. or i.c.v.). Since AAV approach is known to provide sustained transgene expression over time, ³⁸ and the CSF was only collected at the terminal time point for the AAV groups (Table S2), an extrapolated monthly exposure was calculated assuming continuous expression based on the Cmax measured at day 28 (Table S3). Assuming a sustained expression, AAV-delivered vmAb is expected to provide 2-to 7-fold higher monthly exposure in biofluids compared to a high-dose (60 mg/kg) mAb treatment (Table S3).

Next, to assess the location of vmAb versus mAb in various brain compartments, tissues were collected at Cmax (day 1 for mAb and study termination for vmAbs), processed for immunohistochemistry (IHC), and incubated with an anti-human IgG detection antibody (Figure 5C). At the Cmax serum concentration, i.e., 24 h after i.p. administration, the mAb localized in blood capillaries (Ref mAb; Figures 5C and S9) and not within the brain parenchyma, in line with poor penetration across the blood-brain barrier. 39,40 At 28 days post-administration, and consistent with the serum exposure, no mAb was observed throughout the brain sections (data not shown). In contrast, at the peak serum concentration of vmAb (28 days post-administration), striking labeling was observed within cells of the brain parenchyma, with robust expression near the ventricle following i.c.v. administration and within the cerebellum following i.c.m. injection (Figure 5C). Notably, diffuse staining in both AAV-treated mouse cohorts demonstrated broad vmAb distribution throughout the brain. Importantly, the nuclei of the expressing cells appeared white (Figure 5C, white arrows), indicating no nuclear accumulation of vmAb, where the endogenous TDP-43 is predominantly present. This observation suggests that vmAbs are restricted to organelles involved in the secretion pathway, as expected. Additionally, an independent in vitro experiment confirmed that the treatment of human-derived SH-SY5Y cells with AAV9-CBh-ACI-5891 did not alter the generation of relevant splicing variants, thus validating the integrity of TDP-43 functions in producing cells (Figure \$10). In contrast, reduction of TDP-43 levels using a TDP-43-specific short hairpin RNA (shRNA) as control triggered mis-splicing of STMN2 and POLDIP3v2 RNA targets (Figure S10). Taken together, these data demonstrated that the AAV9-mediated vmAb drives safe and sustained expression of functional antibody in adult mice, with local expression in the brain, offering a promising alternative to traditional passive immunotherapy.

A single dose of AAV9-delivered ACI-5891 vmAb potently inhibits the neuropathology induced by patient brain-derived TDP-43 seeds in mouse model

As the mAb, ACI-5891, has been previously reported to inhibit TDP-43-mediated neuropathology, ¹⁴ the AAV9-delivered vmAb was investigated using the same model of human pathology (CamKIIa-hTDP-43NLSm mice). ⁴¹ Following doxycycline removal to induce the hTDP-43NLSm expression, the AAV9-ACI-5891-mIgG2a-treated mice (mixed-sex cohorts) were stereotactically injected

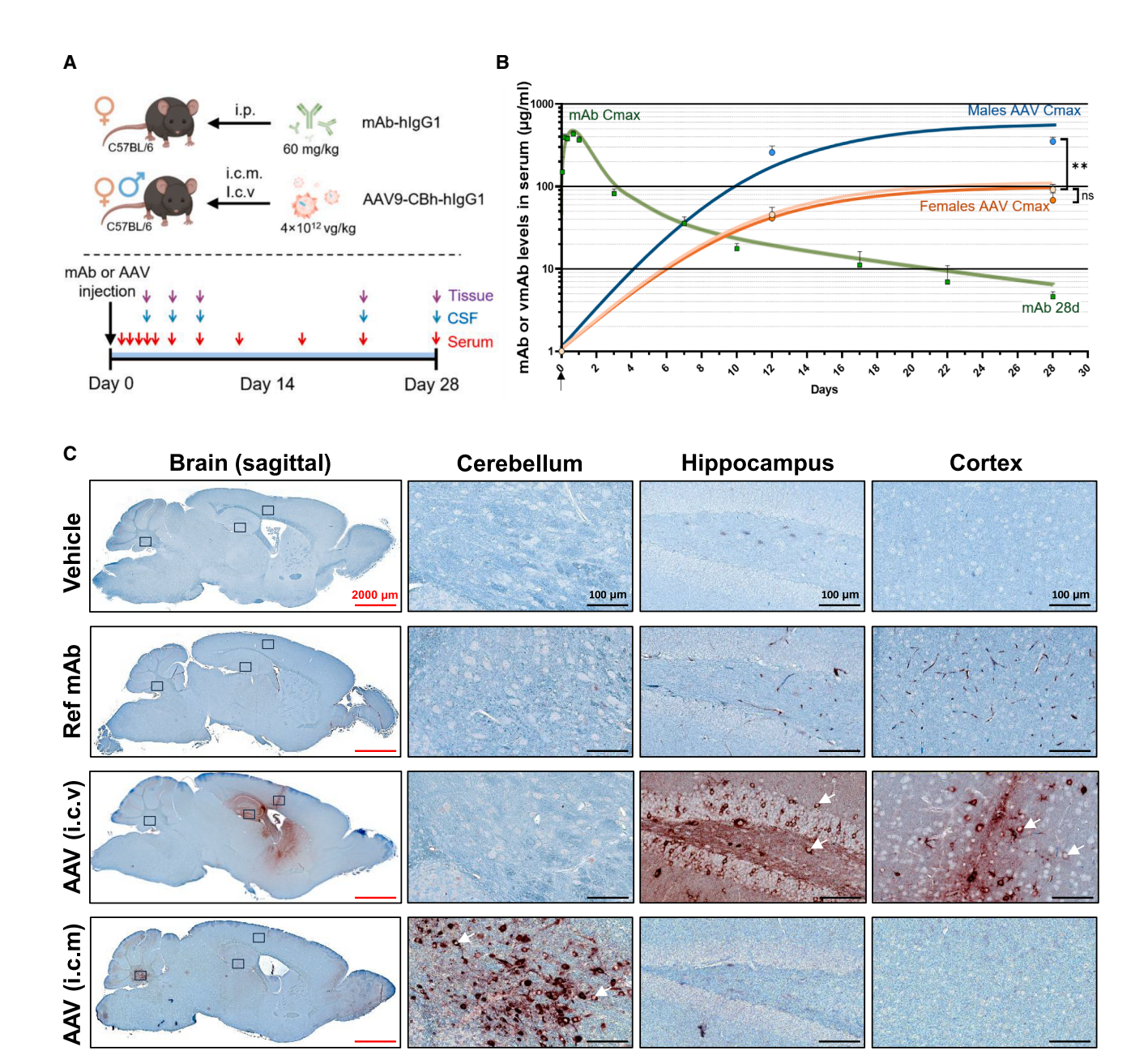


Figure 5. Exposure and localization of ACI-5891 as a mAb versus a vmAb post-administration to mice

(A) Schematic representation of the *in vivo* study design to assess exposure and localization of mAb and vmAb over 28 days. Female and male C57BL/6 mice were administered a single dose of the reference ACI-5891 hlgG1 mAb (Ref mAb) or AAV9-CBh-hlgG1 (encoding for ACI-5891 vmAb). Female C57BL/6 mice (N = 15) received a bolus mAb intraperitoneal administration (i.p., 60 mg/kg) at day 0. The serum was collected at 0.04, 0.17, 0.33, 0.6, 1, 3, 7, 10, 17, 22, and 28 days. The mice (N = 15) were grouped in sub-cohorts (N = 3) to allow staggered serum, CSF, and tissue collections. In the AAV groups, female C57BL/6 mice (N = 15) and male (N = 15) received a single intracerebroventricular (i.c.v.) or intracisternal (i.c.m.) dose of AAV9-CBh-hlgG1 (N = 15) male (N = 15) made 28, while cerebrospinal fluid and brain samples were collected at the study's end (28 days). (B) Levels of Ref mAb ACI-5891 (green) and vmAbs (orange for females and blue for males) in sera over the 28-day period indicate drug exposure. For females, vmAb levels are shown in light orange for intracisternal and dark orange for intracerebroventricular administration. Both mAb and vmAb levels were quantified in sera using a TDP-43-based ELISA. Data are shown as mean (SD); ordinary two-way ANOVA followed by a Tukey's test for multiple comparisons, reported as ** $p \le 0.084$. (C) Sagittal brain sections were immunolabeled with anti-hlgG1-HRP for localization of the mAb or vmAb. Representative images, including magnifications of the cerebellum, hippocampus, and cortex, are provided from mice that were injected with vehicle (i.c.v.)—AAV9 encoding an irrelevant mouse vmAb (top panels); Ref mAb (i.p.)—conventionally CHO-produced reference hlgG1 mAb ACI-5891 administered intraperitoneally, brain collected at the Cmax of serum levels (i.e., 24 h; 2nd panels); and AAV9-hlgG1 administered i.c.v. and i.c.m.—encoding ACI-5891 vmAb, brains collected at study terminantly present. Red scale bar, 2,000 µm; black scale bar, 100 µm.

Table 1. Exposure of ACI-5891 mAb and vmAb in serum and CSF over 28 days after a single drug administration

Test article (sex, route of administration, <i>N</i>)	Serum ^a (μg.mL ⁻¹ .day)	CSF ^a (ng.mL ⁻¹ .day)
mAb-hIgG1 (female, i.p., $N = 15$)	1,281	3,885
AAV9-CBh-hIgG1 (female, i.c.m., $N = 3$)	1,347	-
AAV9-CBh-hIgG1 (female, i.c.v., $N = 3$)	1,101	_
AAV9-CBh-hIgG1 (male, i.c.v., N = 3)	6,395	_

^aValues reported for the area under the curve (AUC) for 28 days calculated from exposure data presented in Figure 5B. AUC has been calculated using the trapezoid rule model in Prism 10.

with human FTLD-TDP brain extracts in the hippocampus to initiate the pathology (i.e., phosphorylated TDP-43 or pTDP-43, Figure 6A). As the study lasted 4 months, the mouse version of the vmAb was used to avoid inducing unwanted immune responses (i. e., anti-drug antibodies, ADAs). The ubiquitous CBh promoter and the astrocyte-selective eGFAP promoter were both assessed to determine the optimal in vivo therapeutic paradigm. Here, a single intracisternal administration was selected due to its safety, tolerability, and extensive evaluation in clinical trials. 42,43 i.c.v. administration was also avoided to minimize efficacy bias resulting from vmAb expression near the FTLD-TDP brain extract injection site within the hippocampus. To assess potential neuroinflammation following AAV administration, we analyzed the microglial marker Iba1 in the hippocampus and cortex. Four months post-AAV administration, no significant differences in Iba1 signal were observed between non-injected controls, vehicle-treated mice, and AAV9treated groups, indicating an absence of microglial activation (Figures S11A-S11C). These findings support the tolerability and favorable safety profile of our approach. VmAb titers were measured in serum and CSF at 4 months post-single-intracisternal administration (Figures 6B and 6C, respectively), confirming sustained expression in both sexes. Both the CBh and eGFAP promoters yielded significant vmAb serum titers at 4 months, ranging from 26 to 490 μg/mL (mean of 200 μg/mL; Figure 6B). For the vmAb titers in CSF, AAV9-CBh versus AAV9-eGFAP ranged from 63 to 504 ng/mL and 35 to 1,214 ng/mL, respectively. The mean value reported for both sexes are 200 ng/mL for AAV9-CBh and 400 ng/mL for AAV9-eGFAP (Figure 6C). As expected, when separating the data based on sex, males consistently had higher serum and CSF titers compared to females (Figure S12), contributing to the variability of the vmAb expression observed in Figures 6B and 6C.

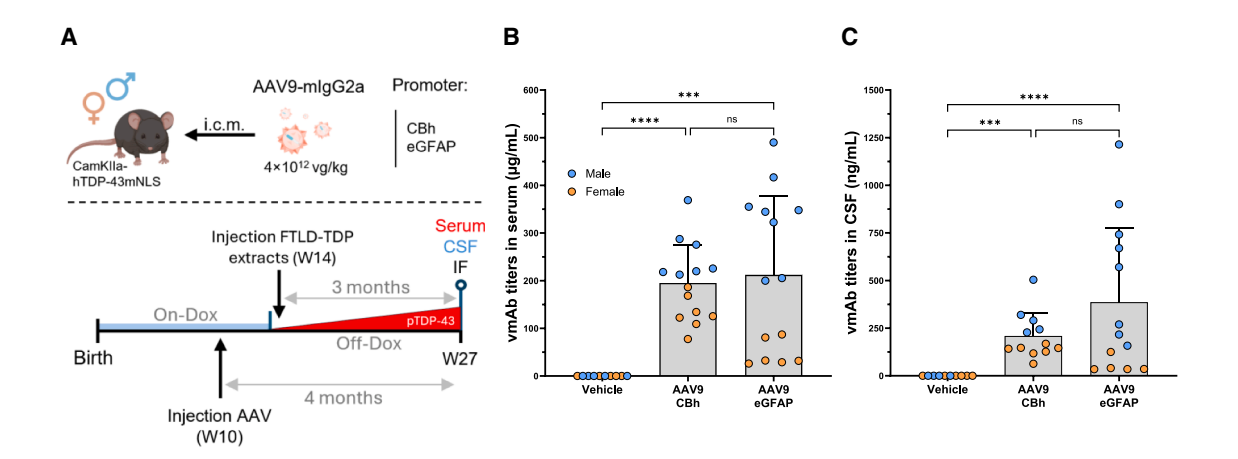
In terms of pathology, significant pTDP-43 accumulation was observed in the ipsilateral hippocampus of vehicle control-treated mice (vehicle) compared to non-FTLD-TDP inoculated mice (no extracts, Figure 6D), consistent with previous report of rare pTDP-43 inclusions. ⁴⁴ For the two AAV-treated mice cohorts, significant reduction of pTDP-43 signals was observed (AAV9-CBh and eGFAP panels, Figure 6D). To ensure that the reduction in pTDP-43 signal was not mistakenly attributed to neurodegeneration (i.e., death of neurons leading to lower levels of pathological TDP-43), pTDP-43

levels were normalized to the staining density of neuronal nuclear protein (NeuN) neuronal marker across all animals evaluated. No significant differences in NeuN count density were observed between the no-extract, non-treated, and treated groups (Figures S13A and S14B). In this study, a single dose of AAV9-mediated vmAbs, driven by either the CBh or eGFAP promoter, significantly reduced pTDP-43 signals by 58% and 68%, respectively, compared to the vehicle control cohort (Figure 6E). Notably, this reduction was independent from the sex of the animals (Figure S14), suggesting that target saturation is already achieved in females despite their lower vmAb expression levels, with no additional efficacy observed at the higher expression levels reached by males. The lack of correlation between exposure and efficacy is shown in Figures S15A and S15B, for serum and CSF, respectively. To our knowledge, this is the first report to show that a vectorized full-length antibody targeting TDP-43 ameliorates neuropathology in a mouse model of ALS/FTD, while confirming the therapeutic potential of C-terminal anti-TDP-43 mAbs reported recently.14,45

DISCUSSION

Vectorized antibodies delivered using AAV technology hold great promise as the next generation of treatments for a plethora of diseases, especially those affecting the CNS. Achieving sustained, high-quality transgene production is crucial for providing safe and effective vectorized immunotherapies. Sustainability is particularly important given that the capsid proteins of AAV vectors elicit humoral responses, preventing patients from accessing future AAVbased treatments after being dosed once. 46-48 To address these issues, we have developed an AAV-antibody delivery system that results in strong expression levels of vmAbs with the quality, binding, and functional properties of a conventionally produced mAb. The breakthrough involved use of a bicistronic IRES expression cassette with the LC gene positioned before the HC that resulted in superiority over previously published vectorized systems including the 2A-based design. 38,49 In vivo, using a single intracisternal injection, these AAV9-delivered vmAbs resulted in a sustained antibody expression for up to 4 months, reaching concentrations of 490 μg/mL in serum and 400 ng/mL in CSF. When using the CamKIIa-hTDP-43NLSm mouse model of ALS/FTD, the single dose of the TDP-43 targeting vmAb ACI-5891 significantly reduced pathological TDP-43 species during the 3-month study period. Importantly, the beneficial effects observed were achieved without perturbing the physiological functions of TDP-43, providing a safety rationale for AAV-delivered anti-TDP-43 immunotherapy.

Successfully expressing full-length mAbs as a vectorized protein has challenged the field to work within the packaging size limitation (4.7 kb) of an AAV expression cassette. Exceeding this maximal capacity poses a significant hurdle to the AAV production yield and impacts crucial manufacturing quality attributes such as the empty/full capsid ratio. Thus, most approaches utilize smaller antibody fragments (e.g., scFv) that unfortunately exhibit substantially weaker target affinity as well as poor stability making them suboptimal for the intended long-term use provided by the



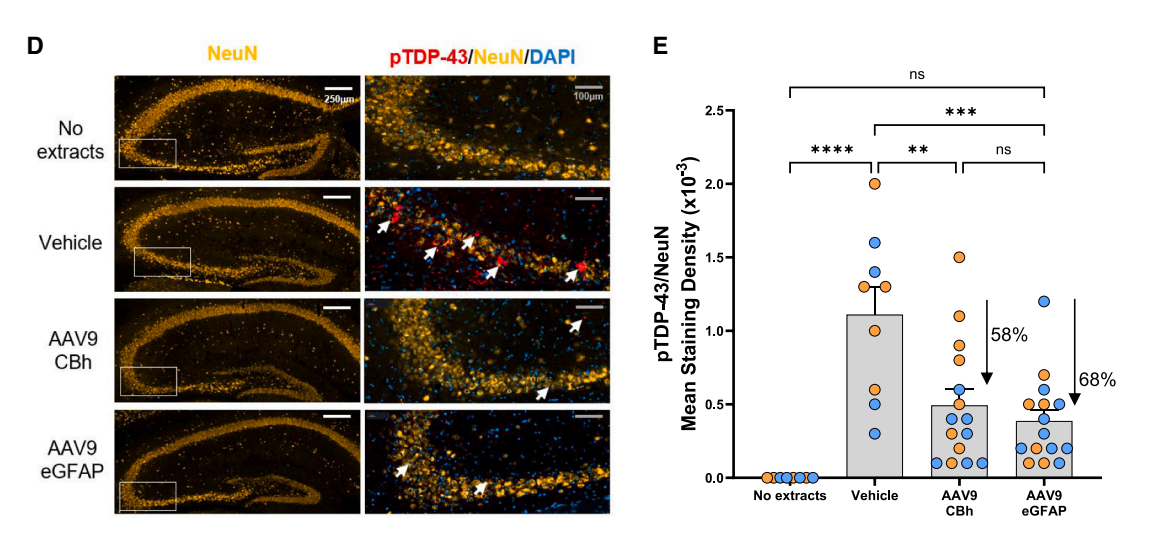


Figure 6. Efficacy of anti-TDP-43 AAV9-delivered vmAb in an ALS/FTD model

(A) Schematic representation of the in vivo study design to assess efficacy of AAV9-delivered vmAb in a CamKlla-hTDP-43NLSm ALS/FTD model. Mice (mixed sexes) were kept on doxycycline (on-dox) until 13 weeks of age. Removal of doxycycline (off-dox) allows expression of human TDP-43 in excitatory neurons. FTLD-TDP extracts were injected unilaterally in dorsal hippocampus 1 week after dox withdrawal (W14). Mice were administered a single dose of AAV9-mlgG2a (encoding for anti-TDP-43 ACI-5891 vmAb) at W10 to allow time for expression. Serum, CSF, and brain tissues were collected at W27, 3-month post-FTLD extract inoculation and 4 months post-single dose AAV injection. (B) vmAb levels in serum and (C) in CSF of CamKlla-hTDP-43NLSm mice, at 4 months post-single-dose administration of AAV9-mlgG2a using either CBh or eGFAP promoters. VmAbs levels are displayed in orange and blue circles, for female and male, respectively. VmAbs were measured in serum and CSF using a TDP-43-based ELISA (μg/mL for serum and ng/mL for CSF, y axis). Data are shown as mean (SD); Kruskal-Wallis followed by a Dunn's test for multiple comparisons, reported as ***p ≤ 0.0003 and ****p < 0.0001. (D) Images of NeuN, pTDP-43, and DAPI immunostaining from ipsilateral hippocampus (inoculated hemisphere) of treated mice, 3 months post-FTLD-TDP extract injection. The left panel shows a low-magnification view of the hippocampus, while the right panel presents a higher-magnification of the area outlined by the white rectangle. The top row ("No extracts") represents mice that were not inoculated with FTLD-TDP extracts, serving as a baseline control for pathology initiation. Vehicle control, AAV9_CBh, and AAV9_eGFAP groups were inoculated with FTLD-TDP extracts to induce pathology. Vehicle-treated mice were intracisternally administered a single dose of CSF mimicking solution. AAV9_CBh and AAV9_eGFAP encode for the mouse IgG2a anti-TDP-43 ACI-5891 vmAb, driven by ubiquitous or astrocyte-selective promoters, respectively. NeuN (yellow) labels neurons, pTDP-43 (red) indicates pathological pTDP-43 inclusions, and DAPI (blue) stains nuclei. White scale bars, 250 µm or gray scale bars, 100 µm for the magnified images (B-D). (E) pTDP-43 staining density normalized to NeuN-positive neuron density in the hippocampus of the mice inoculated with human FTLD-TDP extracts and treated with vehicle control, AAV9-CBh-mlgG2a, or AAV9-eGFAP-mlgG2a. "No extracts" represents mice that were not inoculated with FTLD-TDP extracts and not treated. Data are shown as mean (SD); ordinary one-way ANOVA followed by a Tukey's test for multiple comparisons, reported as **p \leq 0.0020, *** $p \le 0.0003$, and ****p < 0.0001.

AAV-based delivery. 18,51-62 Indeed, these poor biophysical properties of scFv-based fragments were also observed in our study, highlighting the need for alternative solutions. Antibody formats such

as Fab (fragment antigen-binding) are known for their robust stability, ^{63,64} but they do not allow the use of antibody Fc-mediated effector functions, which harnesses the immune system to

eliminate the target-antibody complex from the tissue.⁶⁵ Therefore, the approach reported here, which enables the expression of full-length, high-quality vmAbs, represents a significant advancement in the field.

The use of 2A self-cleavage peptides fused to a protease recognition site enables high full-length antibody expression by ensuring equimolar translation of the HCs and LCs. 66-69 However, improper cleavage of the resulting proteins remains a challenge, compromising protein quality and increasing the risk of a neutralizing immunogenic response. 16,67,70-72 To address these limitations, significant efforts have focused on optimizing self-cleavage sequences to enhance cleavage fidelity and mitigate these risks. Examples include the optimized F2A sequence used in this study⁴⁹ and other peptides such as P2A, T2A, and E2A. 70,73 In contrast, the IRES approach requires careful consideration of gene positioning within the bicistronic expression cassette due to the reduced efficiency of IRES-dependent downstream gene expression.⁷⁴ In the present study, the LC of the antibody was positioned prior to the HC, 20,75 yielding high expression while providing quality comparable to a conventionally produced mAb, offering a notable improvement over gold standard 2A methods.

In vivo, we used a single intracisternal administration of AAV9 wild-type (WT) serotype to closely mimic a potential clinical setup. Given the rapid CSF turnover in mice (30 min, compared to \sim 6 h in humans), ^{76,77} AAV vectors quickly reach the periphery via the blood-CSF barrier. Consistent with previous reports, ^{78,79} AAV9 transduces peripheral tissues, particularly the liver, even though this serotype is largely used for its favorable tropism for cells of the CNS including neurons, astrocytes, oligodendrocytes, and microglia. ^{80–82} A substantial proportion of vmAb is then also produced from the periphery, which may still contribute to CNS exposure similar to a conventional mAb (\sim 0.1%).

The observation of higher levels of vmAb expression in the sera and CSF of male compared to female mice was initially unexpected. However, previous studies have shown that hepatocytes of male mice are more efficiently transduced by WT AAV serotypes, as compared to female mice. ^{34–37} To ensure CNS expression, we conducted thorough *in vitro* and *in vivo* immunochemistry studies. Evaluating expression of the vmAb ACI-5891 using primary cells from rat cortical culture provided the first evidence of successful transduction. After intracisternal or intracerebroventricular administration of the treatment, the cellular morphology and pattern of expression suggested that vmAb production localized in glia cells, neurons, as well as adjacent Purkinje neurons of the cerebellum.

Together, these data confirm local expression of vmAb within the CNS and suggest production in peripheral organs such as the liver, contributing to the difference of expression in male and female as described by Davidoff et al.³⁵ These results have two significant implications for clinical use. (1) Local production of a secreted antibody by glial cells and neurons occurs without signs of neurotoxicity

and neuroinflammation, and the mice remained healthy throughout studies. (2) A single administration obviates the need for bimonthly/ monthly infusions of high-dose immunotherapies. Future improvements in delivery could involve engineered capsids that offer enhanced brain penetration, improved transduction efficiency, and reduced tropism for peripheral organs allowing systemic administration of vectorized antibodies. The use of cell-specific or inducible promoters combined with microRNA target sites for selective transgene silencing in off-target tissues can further elevate next-generation AAV capsids, advancing AAV therapies toward best-in-class precision medicine. ⁸⁶

The advantage of local production by cells from the CNS is further supported by the vmAb CSF-to-plasma ratio observed with the two promoters. Notably, the CSF-to-plasma ratio was higher with the eGFAP promoter compared to the CBh promoter, which correlated with the higher reduction of pathological TDP-43 in the mouse model of ALS/FTD with the AAV9_eGFAP treatment. Unfortunately, the use of the mouse IgG2a version of ACI-5891, which was necessary to avoid ADA responses during the 4-month study, prevented us from performing immunodetection of vmAb in brain tissue to confirm this hypothesis (high background signal from circulating mouse IgG).

Comparing mAbs with vectorized mAbs in preclinical studies presents unique challenges due to differences in pharmacokinetics and expression dynamics. While systemic mAbs reach Cmax within 24 h, vmAbs require 4-8 weeks to reach both Cmax and sustained expression. In fast-progressing mouse models or short-term study designs, this delay limits the ability to postpone treatment initiation relative to disease onset (e.g., doxycycline induction and seed inoculation). The vmAb derived from ACI-5891 showed high affinity for TDP-43 ($K_D \sim 100$ pM), achieving maximal target occupancy at ${\sim}150$ ng/mL in CSF (1,000 pM), well above TDP-43 levels in human CSF (42-163 pM).^{87,88} Interestingly, although female mice have a lower vmAb expression compared to males, this did not result in a significant difference in phospho-TDP-43 reduction. These data suggest that target saturation already may be achieved at lower doses than theoretically calculated or that parenchymal production of the antibody could lead to a higher effective concentration within the brain tissue, extending beyond CSF exposure alone. These insights highlight the need for sex-specific considerations in optimizing preclinical models and clinical strategies, including the potential for dose adjustments to enhance safety while maintaining sufficient therapeutic efficacy.

Together, the bicistronic IRES system represents a significant advancement over traditional 2A methods, offering a better alternative for clinical applications. The present work is the first to show efficacy of a vectorized full-length antibody targeting extracellular TDP-43 that inhibits neuropathology in a model of human neurodegenerative disease. While validating the potential of developing an immunotherapy to target extracellular TDP-43-driven pathology in patients, ¹⁴ it also confirmed the potency of the anti-TDP-43

ACI-5891 mAb, with the added advantage of a single-dose administration. Achieving such a significant reduction of pathology using an AAV9 WT serotype, we anticipate that further improvement could be achieved using engineered AAV vectors. Ours and future innovative approaches are desperately needed to address these devastating diseases that impose such a high burden on patients, families, and society.

MATERIALS AND METHODS

CHO cell transfection

CHO transfections were performed using the ExpiCHO transient expression system (Thermo Fisher Scientific, USA) and 24-deepwell plate with rectangular well (Corning, USA), according to the supplier protocol. In brief, triplicates of 2.5 mL cells per well (5 \times 10^6 cells/mL) were transfected each with 1 µg/mL plasmid mixed to OptiPro complexation medium supplemented by ExpiFectamine and grown for $\sim\!18$ h at 37°C, 8% CO₂, under 200 rpm rotation shaking. After that, cells received 600 µL of feed solution per well supplemented by ExpiCHO enhancer to reach a final volume of 3.1 mL per well. The temperature was lowered to 32°C, and cells were grown until harvest (7–12 days).

Molecular biology and AAV generation

Gene constructs and plasmid components were designed by AC Immune. VectorBuilder, China, produced the plasmid constructs, performed DNA sequencing, and produced AAV capsids within an ultra-purified quality grade, purified by cesium chloride density gradient as described by Ayuso et al.⁸⁹ In the case of furin/2A constructs, we used the sequence described by Fuchs et al. (2016) aiming an optimal protein maturation.⁴⁹ Functional sequence of human OLIG2 promoter was identified using the EPFL (Ecole polytechnique fédérale de Lausanne) promoter database. 32,33 CBh (hybrid form of the chicken beta-actin promoter [CBA]) and human short GFAP (glial fibrillary acidic protein) promoter sequences were subcloned as described by the authors.^{31,90} CMVe (cytomegalovirus promoter enhancer) sequence that is part of the cytomegalovirus (CMV) promoter⁹¹ was subcloned directly on the 5' end of both OLIG2 and short GFAP promoters to generate eOLIG2 and short eGFAP, respectively. Related to mAb and vmAb design, the original mouse variable heavy (VH) and variable light (VL) sequences from the murine hybridoma were recombinantly cloned onto mouse IgG2a constant region (UniProt: P01863) and mKappa constant region (Uni-Prot: P01837), respectively. The hIgG1 chimeric antibody (hIgG1) was generated by grafting the murine VH and VL regions onto the hIgG1 and hKappa constant region, respectively (UniProt: P01857 and UniProt: P01834). A list of annotated sequences corresponding to the various proteins and expression cassettes, including the control trastuzumab and mouse-derived sequence, is provided in the supplementary material (Tables S4 and S5).

Antibody titration in CHO cell supernatant

One hundred microliter samples were collected per clone in triplicate and then centrifuged at 800g for 2 min at room temperature (RT) in microfuge tubes. Supernatants were transferred to fresh

tubes, and titers were determined for each triplicate supernatant using bio-layer interferometry (BLI) on the Octet QKe system (Sartorius, Germany). Protein A biosensors (Sartorius, Germany) were used to quantify full-length vmAb and scFv-Fc. For all measurements, a standard curve was generated using the corresponding purified protein, previously produced in CHO cells with two plasmids (one per antibody chain) and purified by standard methods. The assay buffer was PBS supplemented with 0.1% BSA and 0.02% Tween.

Protein purification

Triplicate samples from each clone were pooled to obtain ~ 9 mL per clone. Cells were pelleted by centrifugation at 800g for 2 min at RT, and the supernatants were transferred to fresh 15 mL Falcon tubes. Three hundred microliters of protein A resin (Cytiva, USA), equilibrated in PBS, were added to the 9 mL IgG and scFv-Fc clone supernatants. The samples with resin were gently rotated for 30 min at RT to ensure uniform mixing and efficient protein capture.

Following incubation, tubes were centrifuged at 3,000g at RT, and supernatants were discarded. The resin was then washed twice with PBS buffer. The resin-captured IgG and scFv-Fc were resuspended in 1 mL 100 mM glycine with pH 2.8 supplemented by 100 mM NaCl. The solution containing eluted antibody was transferred to a 1.5 mL microfuge tube and centrifuged at 20,000g for 5 min at 4°C. Supernatants were collected and immediately neutralized with 200 μ L of 1 M Tris-HCl, pH 7.6. Finally, protein concentrations were determined by measuring absorbance at 280 nm using the appropriate extinction coefficient for each protein.

Protein characterization by SDS-PAGE

Purified proteins (1 μg , unless otherwise specified) were denatured for 5 min at 95°C in loading buffer, with or without the addition of 5 mM dithiothreitol. The samples were then separated on a 4%–12% gradient SDS-PAGE gel, followed by Coomassie blue staining to visualize assembled IgGs ($\sim\!150$ kDa) and the respective reduced LCs ($\sim\!25$ kDa) and HCs ($\sim\!50$ kDa). For scFv-Fcs, the non-reduced protein migrated at $\sim\!110$ kDa, while in reduced conditions it migrated at $\sim\!60$ kDa.

Protein characterization by SEC

Purified mAbs, vmAbs, and scFv-Fc were separated by fast protein liquid chromatography on a Superdex Increase S200 10/300 GL column (Cytiva, USA) using an Äkta system (Cytiva, USA). The separation was performed at 4°C in PBS buffer, running 1.2 column volumes at a flow rate of 0.7 mL/min. UV absorbance at 280 nm was used to monitor protein elution, and the monomeric protein fraction was calculated by determining the ratio of the monomer peak area to the total chromatogram area.

Primary protein sequence analysis by mass spectrometry

Recombinant primary protein sequences were analyzed by mass spectrometry (MS) at the Proteomic Core Facility, EPFL, Lausanne, Switzerland. First, 5 µg of purified protein samples was separated by

SDS-PAGE under reducing conditions as described earlier. After that, resulting SDS-PAGE was incubated in ultra-purified water at RT, for 2 h under gentle shaking, and then stained with Coomassie blue. In brief, stained protein bands corresponding to the LC and HC were excised and transferred to fresh 1.5 mL tubes. Gel pieces were washed twice with 50% ethanol in 50 mM ammonium bicarbonate (Sigma-Aldrich) for 20 min and dried by vacuum centrifugation. Proteins were reduced with 10 mM dithioerythritol (Merck Millipore) for 1 h at 56°C followed by a washing-drying step as described earlier, and reduced disulfide bonds were alkylated with 55 mM iodoacetamide (Sigma-Aldrich) for 45 min at 37°C. The iodoacetamide was removed, and the gel excisions were washed with ultra-purified water, followed by in-gel digestion overnight at 37°C using MS grade trypsin (Pierce) supplemented by 10 mM CaCl₂. The resulting peptides were resuspended in 2% acetonitrile (Biosolve) and 0.1% formic acid (Merck Millipore) for the LC-MS/MS separations. Peptides sequences were then identified, and primary sequence analyzed for integrity.

Cell transduction by AAV

Either ExpiCHO-S, SH-SY5Y cells or rat primary cortical culture were transduced with AAV constructs using an MOI (multiplicity of infection) ranging from 100K to 130K (100.000 or 130.000 vg per cell). AAV constructions were diluted in the respective cell media to reach the calculated MOI required for the transductions and added directly to plate wells. Cells were then grown for days at 37°C and 5% CO₂ according to the cell line viabilities. Supernatant was collected either for purification of secreted vmAb, SEC characterization, or binding experiment performed by ELISA as described in the following.

Affinity measurements to human TDP-43

Target binding affinities were performed on a Biacore 8K instrument (Cytiva). Recombinant soluble human TDP-43 (Selvita) was immobilized on flow cells 2 (fc 2) of channels 1 to 8 of a series S CM5 sensor chip (Cytiva) to reach 350 to 450 RU (resonance units) on all eight channels. Five successive increasing concentrations of recombinant mAbs ranging from 1.2 to 100 nM prepared from a 3-fold serial dilution in PBS containing 0.05 % surfactant Tween20 (PBS-P+, pH 7.4) running buffer were injected in single-cycle kinetics on fc 1 and fc 2. Kinetic measurements were performed with a contact time of 300 s and a dissociation time of 3,600 s at a flow rate of 30 μ L/min. Regeneration was performed using one injection of 10 mM glycine-HCl pH 1.7, at a flow rate of 30 μ L/min for 30 s.

To assess the binding properties of the *in vivo*-produced vmAb, another SPR setup was developed. First, an anti-human IgG antibody from the Human Antibody Capture Kit, type 2 (Cytiva), was immobilized on fc 1 and fc 2 of a series S CM5 sensor chip (Cytiva) using amine coupling, following the manufacturer's recommendations. This immobilized antibody was then used to capture hIgG1 vmAbs and mAbs present in mouse serum from the study described in Figure 5A. Next, mouse serum was diluted approximately 100-fold in PBS-P+ buffer (pH 7.4) containing 10 mg/mL non-specific bind-

ing reducer (NSB reducer, Cytiva) to achieve a final concentration of 3 μg/mL of anti-TDP-43 mAb and vmAb, as quantified by the TDP-43 ELISA. The resulting diluted serum was injected on fc 2 at a flow rate of 5 µL/min to capture in vivo-produced human vmAb and Ref mAb at levels ranging from 221 to 308 RU. Single-cycle kinetic analysis was performed by injecting successively five increasing concentrations of soluble recombinant full-length human TDP-43 (Selvita) prepared in PBS-P+ (pH 7.4) running buffer. The concentrations ranged from 1.2 to 100 nM. Binding kinetics were measured using a contact time of 300 s and a dissociation time of 900 s at a flow rate of 30 µL/min. Regeneration was achieved through an injection of 10 mM glycine-HCl (pH 1.5) at a flow rate of 30 μ L/min for 60 s. Results obtained from single-cycle kinetics were double-referenced using the reference fc 1 and preceding blank cycle for evaluation with the Biacore Insight evaluation software. Sensorgrams were analyzed using the 1:1 Langmuir kinetic fit model with variable reflective index and global Rmax parameters.

TDP-43 aggregation assay in vitro

The method was adapted from Afroz et al. 14 The recombinant human TDP-43 protein was expressed with a C-terminal fusion to the maltose binding protein (TDP-43-MBP), incorporating a TEV protease cleavage site for potential removal of the MBP tag. This fusion protein was produced in Escherichia coli (E. coli), purified, and aliquoted before storage at -80° C (Selvita, Poland). Storage buffer (20 mM Tris-Cl pH 8.0, 300 mM NaCl, 5% glycerol, and 1 mM DTT) was exchanged against assay buffer (30 mM Tris and 150 mM NaCl, pH 7.4) using centrifugal filters. The protein concentration was determined by UV spectroscopy at 280 nm. TDP-43-MBP was diluted in assay buffer to a final concentration of 2.5 µM and mixed in low binding tubes with 600 nM of anti-TDP-43 Ref mAb (mIgG2a ACI-5891), IRES_mIgG2a mAb (produced using bicistronic expression cassette), or irrelevant isotype control. Aggregation of TDP-43 was induced by addition of TEV protease at a final concentration of 10 µg/mL. Protein aggregation was monitored by measuring absorbance at 600 nm in the center of each well. Measurements were taken every 15 min over a 24 h period, with 5 s of shaking before each measurement (Tecan, Switzerland). The sealed plates were constantly kept in the plate reader at 25°C, and all measurements were performed in technical triplicates to ensure reproducibility (n = 2). To ensure complete cleavage of TDP-43-MBP by the TEV protease in the presence of anti-TDP-43 mAbs, 4 µL of samples were mixed with 1 µL 5× fluorescent mastermix (Bio-Techne, USA) and analyzed by capillary electrophoresis (Jess, ProteinSimple) after 24 h incubation. An anti-C-terminal TDP-43 antibody labeled with DyLight 680 was used as primary detection antibody at 20 μg/mL.¹⁴ For analysis, endpoints measured by absorbance after 24 h were normalized to isotype control, and the percentage of aggregated TDP-43 calculated for each conditions.

IF on human postmortem brain sections

Frozen human postmortem tissues were obtained from the brain banks affiliated with the University of California, San Francisco (UCSF). All tissues were collected from donors from whom a written informed consent for a brain autopsy and the use of the material and clinical information for research purposes had been obtained by the respective institution. All samples were anonymized and coded. The brain samples were cut at 10 μm thickness, mounted on microscope slides, and stored at $-80^{\circ} C$ until further use.

Frozen brain sections were thawed at RT, fixed with 4% paraformaldehyde (PFA) at 4°C for 15 min and washed 3 times with PBS. Tissues were then encircled with a hydrophobic pen to minimize the sample volume and avoid spreading. Blocking was performed with 5% BSA in PBS with 0.25% Triton X-100 for 1 h at RT. The sections were incubated overnight at 4°C with primary antibody mAb ACI-5891 or IRES_mIgG2a ACI-5891 at 1 μg/mL and pTDP-43 (s409/ 410) antibody (BioLegend, USA) at 1:200 diluted in 2.5% BSA in PBS-0.25% Triton X-100. To assess background signals from the secondary detection antibody, the primary antibody was replaced with buffer (Neg control). The next day, the sections were washed 3 times with PBS. As secondary antibody, Alexa Fluor-633-labeled anti-rat and Alexa Fluor 488-labeled anti-mouse or Cy3 anti-human diluted 1:500 in PBS were used. The sections were incubated in secondary antibodies for 30 min at RT. After three washes with PBS, 0.1% Sudan Black dissolved in 70% ethanol was added to the brain sections for 15 min at RT to minimize auto-fluorescence. After three washes in PBS, ProLong antifade reagent with DAPI was added, and the sections were mounted with coverslips. The brain sections were dried in the dark and imaged with the Panoramic 150 slide scanner using the fluorescein isothiocyanate, Cy5 or Cy3, and DAPI channels.

Rat primary cortical cell culture

The rat pups (Prague-Dawley, Charles River, postnatal day 1-1.5) were sacrificed according to a veterinarian approved protocol. The pups were dissected in a 10 cm dish in Hank's balanced salt solution under the binocular at RT. The brains were kept in a 35 mm dish in MEM (minimum essential medium, Gibco, 12360-038). Brains were transferred into a drop of digestion medium (30 mM K₂SO₄, 90 mM Na₂SO₄, 5.8 mM MgCl₂, 0.25 mM CaCl₂, 1.6 mM HEPES, 0.2 mM NaOH, 0.5% phenol red, 20 U/mL papain, 0.1% [w/v] L-cysteine, and 0.36% [w/v] glucose) and cut in pieces before being transferred into a tube containing digestion medium and incubated 30 min at 37°C. Supernatant was removed, and 10 mL of protease inhibitor medium was added (30 mM K₂SO₄, 90 mM Na₂SO₄, 5.8 mM MgCl₂, 0.25 mM CaCl₂, 1.6 mM HEPES, 0.2 mM NaOH, 0.5% phenol red, 0.36% [w/v] glucose, and 0.1% [w/v] trypsin inhibitor [Sigma, T9253]) and incubated 10 min. The tube was centrifuged at 300g for 2 min at RT, and the supernatant was removed. Tissue was resuspended in 5 mL of trituration medium (10% horse serum [Sigma, H1138], 1% L-glutamine [Gibco, 25030-025], and 0.36% [w/v] glucose in MEM). Trituration was performed using a 5 mL serological pipette and pipetting up and down 10 times. Once all tissue was dissolved, the tube was centrifuged at 300g for 2 min at RT. Supernatant was removed, and cells were resuspended in 10 mL of adhesion medium (10% horse serum, 1% L-glutamine, 1% penicillin/streptavidin, and 0.36% [w/v] glucose in MEM). Cells were passed through a 70 μ m cell strainer. The filter was washed with an additional 10 mL adhesion medium. Cells were counted using a NucleoCounter NC-250 and plated at 25,000 or 40,000 cells/well in 96-well poly-D-lysin-coated plates in 100 μ L. Cells were incubated at 37°C, 5% CO₂. After 4 h, the medium was changed for growth medium (1% L-glutamine, 1% penicillin/streptavidin, and 2% B27 [Gibco, 17504-044] in Neurobasal medium [Gibco, 12348-017]).

IF of rat primary cortical cell culture

Cells were fixed with 4% PFA (Sigma-Aldrich) diluted in PBS for 15 min at RT to preserve cellular structures. After fixation, cells were washed 3 times with PBS to remove residual PFA. Permeabilization and blocking were performed simultaneously in PBS supplemented by 3% BSA and 0.1% Triton X-100 overnight at 4°C. Cells were then washed 3 times with PBS. After that, cells were incubated overnight at 4°C with primary antibodies diluted in a solution of PBS supplemented by 1% BSA and 0.1% Triton X-100. The final volume of antibody solution added was 50 µL per well. Primary antibodies used included anti-MAP2 (Abcam, chicken antibody # ab5392), at a dilution of 1:2,000, to recognize microtubule-associated protein 2 and identify neuronal cells, and anti-GFAP (Merck, rabbit antibody # 5804), at a dilution of 1:5,000, to target glial fibrillary acidic protein and label astrocytes. Following incubation with the primary antibodies, cells were washed three times with PBS to remove unbound antibodies. After washing, cells were incubated with fluorescently labeled secondary anti-antibodies diluted in PBS supplemented by 1% BSA and 0.1% Triton X-100 for 1 h at RT in the dark to prevent photobleaching. Secondary antibodies included Alexa Fluor 488 goat anti-chicken IgG (Thermo Fisher Scientific, #A11039), diluted at 1:500, for the detection of the anti-MAP2 antibody; Alexa Fluor 647 goat anti-rabbit IgG (Thermo Fisher Scientific, # A32733), also diluted at 1:500, to label the anti-GFAP antibody; and Alexa Fluor 555 goat anti-mouse IgG2a (Invitrogen, # A21137) for vmAb detection, diluted at 1:200. Cells were then washed 3 times in PBS buffer as earlier. Finally, cells were stained to visualize cell nuclei using DAPI dye diluted in PBS according to the manufacturer's instructions for 5 min at RT, followed by a final PBS wash. Cells were then imaged using a Leica microscope equipped with a $20\times$ objective lens. All fluorescence imaging parameters were standardized across samples for consistent data acquisition.

Assessment of TDP-43 functionality by quantitative reversetranscription PCR

SH-SY5Y cells were grown at 100K cell per well in 24-well microplates and differentiated in DMEM high-glucose medium (Gibco, 11965092) supplemented with 2% fetal bovine serum (Gibco, 10500064), 1% penicillin-streptomycin (Gibco, 15140122), and 10 μ M retinoic acid (Thermo Scientific Chemicals, 044540.04). Following differentiation, cells were transduced in either duplicates or triplicates with an MOI of 130K of AAV9-vmAb constructs. Cells were then incubated with either an AAV9-delivered shRNA scramble (negative control) or AAV9-delivered shRNA anti-*TARDBP* as a positive control. The shRNA anti-*TARDBP* will reduce TDP-43 levels in cells and thus will affect its function. Cells were also

transduced with 130K MOI of AAVs or treated with 2 µg/mL of mAb ACI-5891 spiked into the cell supernatant. Cell supernatants were removed at day 7 following transduction for further antibody titration by ELISA to ensure production by cells. After that, cells were detached in 100 µL of trypsin solution (TrypLE Express Enzyme, cat# 12563029) and transferred to mRNAse-free (messenger ribonucleic acid-free) microfuge tubes. Cells were pelleted by centrifugation, 5 min at 800g at 4°C. After that, cells were resuspended in lysis buffer, and mRNA was extracted according to GeneJET RNA purification kit recommendations (Thermo Fisher Scientific, cat# K0732). Corresponding cDNAs were then prepared using the Maxima H Minus First Strand cDNA Synthesis Kit as recommended by the manufacturer (Thermo Fisher Scientific, cat# K1651). After that, qPCRs were performed with the QuantStudio 3 real-time PCR system, starting with a single cycle of 2 min at 50°C, then 2 min at 95°C and followed by a total of 40 cycles consisting of 15 sec at 95°C and 1 min at 60°C for the primer hybridization. The collected data were then analyzed with the supplier software, and either duplicate or triplicate cycle thresholds were collected per cell treatment to calculate the \mathcal{Z} - $\Delta\Delta$ Ct, where $\Delta\Delta$ Ct = Δ Ct (treated sample) – Δ Ct (untreated sample). The house keeping gene considered as not affected by TDP-43 activity was human RPLPO. The gene and primers used for the qPCR TDP-43 functionality assay were as follows: (1) STMN2 (fwd) AGCTGTCCATGCTGTCACTG and (rev) GGTGGCTTCAA GATCAGCTC, (2) truncated STMN2 (fwd) GGACTCGGCAGAAG ACCTTC and (rev) GCAGGCTGTCTGTCTCTC, (3) POL-DIP3v2 (fwd) GCTCACCAAAACCATCCAGAA and (rev) ACTG CTTAGCCCAGCCATGT, (4) TARDBP (TDP-43 gene) (fwd) AATTCTGCATGCCCCAGA and (rev) GAAGCATCTGTCTCAT CCATTTT, and (5) RPLP0 (fwd) TCTACAACCCTGAAGTGC TTGAT and (rev) CAATCTGCAGACAGACACTGG.

Detection of vmAb by TDP-43 ELISA

This method was developed to (1) quantify vmAb levels in cell culture supernatants and in vivo biofluids and (2) confirm that AAVdelivered vmAb, whether produced by rat primary cortical cultures or detected in vivo (in serum or CSF), retained its functionality and binding affinity for TDP-43. Ninety-six well microplates (Thermo Fisher Scientific, USA) were coated with human full-length TDP-43 soluble protein (Selvita, Poland) diluted in 50 mM carbonate buffer pH 9.6 at 4°C overnight. The following day, plates were blocked with either 1x PBS + 1% BSA for CSF or supernatant samples or 1x PBS + 5% milk for serum samples (150 μL per well) during 1 h at RT. After blocking, plates were washed three times with 1x PBS + 0.2% Tween 20 (300 µL per well). For the standard curve, conventionally produced reference mAbs (mAb-hIgG1 or mAb-mIgG2a ACI-5891) were prepared at an initial concentration of 1 µg/mL in the appropriate blocking buffer. An 11-point, 1:3 serial dilution was then performed, starting from 1 µg/mL and continuing down to 0.017 ng/mL. Sample dilutions were adapted to reach an optical density (OD) value falling in the linear part of the standard curve. After 1 h at RT, plates were washed three times as previously described. For detection, an anti-mouse IgG2a horseradish peroxidase (HRP) secondary antibody (Abcam, United Kingdom) or an anti-human IgG Fc HRP secondary antibody (Abcam, United Kingdom) was diluted 1/10,000 in 1x PBS + 0.2% Tween 20 and added to the plate (50 μL per well). Plates were incubated for 30 min at RT and washed three times as previously described. TMB substate (tetramethylbenzidine, BD Biosciences, USA) was added at 50 μL per well and incubated 5–10 min at RT. The reaction was stopped with 50 μL per well of 2 M HCl. Absorbance was then read at OD 450 nm using a microplate reader (Agilent, USA). The standard curve was fitted using a four-parameter dose-response curve, and concentrations extrapolated from the equation.

AAV9-mediated vmAb expression in vivo

These studies were performed in accordance with veterinary authorizations and animal care guidelines. Female and male C57BL/6 mice between the ages of 8–12 weeks were used for the studies illustrated in Figures 4 and 5. The animals were sourced from Charles River. For conventionally produced mAb (either Ref mAb ACI-5891 or isotype controls), i.p. injections were performed into lower-right quadrant of the abdomen to avoid damage to the urinary bladder, cecum, and other abdominal organs. Female C57BL/6 mice (N=15) received the bolus mAb administration (60 mg/kg) at day 0. The serum was collected at 0.04, 0.17, 0.33, 0.6, 1, 3, 7, 10, 17, 22, and 28 days. The mice (N=15) were grouped in sub-cohorts (N=3) to allow staggered serum, CSF, and tissue collections.

For the single cisterna magna (i.c.m.) AAV administration, a dose of 1 mg/kg buprenorphine slow release (0.6 mg/mL) was subcutaneously administered to the animal prior to the surgery to provide 72 h of analgesia. AAV injections were performed into the cisterna magna under anesthesia with 2.5% isoflurane. The final volume for i.c.m. injections was adjusted at 10 µL with sterile artificial CSF (prepared from high-purity water and analytical grade reagents; microfiltered and sterile; final ion concentrations [in mM]: Na+ 150; K+ 3.0; Ca2+ 1.4; Mg2+ 0.8; P 1.0; Cl- 155) to decrease the volumeinduced margin of error and to be consistent between animals by injecting an equivalent volume. Briefly, animals were deeply anesthetized with 2.5% isoflurane and placed in the prone position in a stereotaxic head holder, with the head and body at a 120° angle. The skin and muscle at the nape of the neck were retracted. A 36G Hamilton syringe was used to pierce the dura matter at the site of the cisterna magna. The AAV vector was injected at a rate of 1 µL/ min, and the overlying skin was then sutured. Animals were allowed to recover on a warming mat.

i.c.v. injections were performed unilaterally into the left ventricle under anesthesia with 2.5% isoflurane. The final volume for i.c.v. injections was adjusted at 10 μL with sterile artificial CSF. The scalp was shaved, and the skin was prepped using 0.5% chlorhexidine and 70% ethyl alcohol. The animal was placed in a stereotaxic head holder (David Kopf Instruments, Tujunga, CA). The skin was retracted, and the cortical surface of the left hemisphere was exposed by craniectomy using a high-powered drill. Injections were performed with the aid of a microinjection unit (David Kopf Instruments), and a Hamilton syringe was introduced into the left hemisphere

(coordinate: -0.25 mm posterior relative to bregma, left 1.0 mm from midline), located at a depth of 2.5 mm below the skull to target the left lateral ventricle. The AAVs were injected at a rate of 1 μ L/min at a dose of 4 \times 10¹² vg/kg (1 \times 10¹¹ vg in 10 μ L for i.c.m. or i.c.v.)

Upon study termination, the CSF and blood were collected, animals were perfused with 40 mL PBS with 100 U/mL heparin, and organs of interest were collected.

The brain was dissected in the mid-sagittal plane, and the left hemi-sphere was immersion-fixed in 10% neutral-buffered formalin for 72 h. Fixed brain for paraffin embedding was dehydrated through graded ethanol and xylene and then infiltrated with paraffin wax.

Tissue sectioning and immunohistochemistry

Brains were sectioned at 8 µm thickness per section. Slides were stored at RT prior to staining. For immunohistochemistry (IHC) preparation, slides with tissue sections were de-paraffinized and rehydrated on the Leica BOND autostainer, followed by antigen retrieval with citrate buffer at 100°C for 20 min to enhance antigen accessibility. A 5-min incubation with a peroxide block was applied to reduce endogenous peroxidase activity. To prevent nonspecific antibody binding, a solution of SuperBlock (Thermo Fisher Scientific) was applied for 10 min. After blocking, slides were incubated for 1 h with the primary antibody, anti-human IgG (Abcam, ab109489), and a rabbit mAb, at a 1:300 dilution. This was followed by incubation with the labeled polymer provided in the BOND polymer refine HRP plex detection kit for 30 min. Slides were then developed with the chromogen substrate 3-amino-9-ethylcarbazole for 20 min to visualize staining. All stained sections were counterstained with Acid Blue 129 (Sigma-Aldrich) to provide contrast, followed by mounting with PEG (polyethylene glycol)/Glycerol aqueous mounting medium for preservation. Following staining, slides were dried at RT for 48 h before being digitized using an Axioscan 7 digital whole-slide scanner (Carl Zeiss, Canada) to capture highresolution images of each sample.

In vivo efficacy study in CamKlla-hTDP-43NLSm transgenic mice injected with FTLD-TDP brain extracts

Double transgenic CamKIIa-hTDP43-NLSm animals were generated by crossing hemizygous females (JAX Stock # 14650: B6; C3-Tg(tetO-TARDBP*)4Vle/J) with hemizygous males (JAX Stock # 007004: B6.Cg-Tg(CamKIIa-tTA)1Mmay/DboJ). Based on power calculations for histological neuropathology evaluation from other models of neurodegeneration, a group size of N=10-15 was predicted. Additionally, to ensure this number for the final analysis and to allow for a 60%–70% success rate of stereotactic surgery and inoculation of patient brain extracts, the initial group size was defined as N=15 per treatment group and N=11 for the non-treated group. This study was conducted in a mixed sex cohort. No sex-specific differences in the progression of pathology have been described in this model, 41 but significant vmAb expression levels were observed in C57BL/6 WT mice. A total of 52 mixed-sex mice (N=52) were used in this study. Breeders and mice were kept on

200 mg/kg doxycycline (dox) diet until 13 weeks of age. A week after the dox removal from diet (W14), CamKIIa-hTDP-43NLSm mice were deeply anesthetized with isoflurane and immobilized in a stereotaxic frame. Human sarkosyl insoluble extracts were sonicated prior injection in the dorsal hippocampus.⁹² A Hamilton syringe was introduced into the left hemisphere (coordinates relative to bregma: -2.0 mm anterior and left 1.3 mm from midline), using an operating microscope and a microinjection unit (David Kopf Instruments). Three dorsal hippocampus locations were targeted, starting at an initial depth of -1.95 mm below the dura and then partially withdrawing the needle to -1.55 mm for the middle injection, and again to -1.15 mm for the third and final injection. The FTD extracts were injected at a rate of 0.3 µL/min (1.0 µL per site, 3 μ L total volume) with the needle in place for \geq 10 min at each target. The single dose of AAV9 encoding the anti-TDP-43 antibody (mouse IgG2a ACI-5891) was i.c.m. administered, 28 days prior the human sarkosyl insoluble extracts to match peak expression of vmAb reached at 1-month. Terminal collection was performed at 3 months after FTLD-TDP extract inoculation.

Animals were weighed at day 0 and then weekly for the duration of the study. Motor performance was assessed weekly for signs of motor dysfunction, including tremors and clasping. Each sign was scored on a scale of 0–3: normal (no dysfunction) (0), mild (1), moderate (2), or severe (3) dysfunction.

Brain hemispheres subjected to histology were snap frozen and then immersion-fixed in formalin for 24 h. The tissue was then embedded into an optimal cutting temperature matrix and frozen on dry ice with a super-cooled bath of 2-methylbutane. Frozen tissue blocks were sectioned coronally at 20 µm thickness per section. Slides were stored at -20° C prior to IF staining. Staining was performed on a Leica BOND RX. For the dual pTDP-43/NeuN IF staining, the slides initially underwent a fixation/permeabilization step in methanol/acetone (1:1) for 10 min and washed in PBS. Then epitopes were retrieved in Leica ER1 buffer pH6 (AR9640) for 10 min at 100°C, followed by an incubation with Protein Block (PowerVision IHC/ISH Super Blocking, Leica, Ref. PV6122). Slides were then incubated with primary antibodies in two steps, first with anti-pS409-410 TDP-43 (BioLegend, 829901,1/500), followed by anti-NeuN (Millipore, MAB377(CH), mouse antibody (Ab), 1/500). Next, secondary antibodies were incubated in two steps, firstly with a mix of antibodies, anti-mouse-Cy3 (Jackson ImmunoResearch, goat Ab, 1/200) and anti-rat-biotin (Jackson ImmunoResearch, goat Ab, 1/250), and secondly with streptavidin-Cy5 (Jackson ImmunoResearch, 1/300). Iba1 staining was performed using a dilution of 1/1,000 primary rabbit antibody (Wako, Ref. 019-19741), followed by anti-rabbit-Alexa 488 (Jackson ImmunoResearch, goat Ab, 1/200). Finally, slides were incubated with DAPI (1/300). All antibodies were diluted in BOND antibody diluent (AR9352), and slides were mounted in antifade and cover slipped. The IF slides were digitized using an Axio Scan.Z1 digital whole-slide scanner (Carl Zeiss, Canada). Region of interest (ROIs) were delimited using a U-Net convolutional neural network trained on a dataset of manually painted tissue sections. The ROIs then underwent visual quality control (QC) review and were manually adjusted, if needed. Quantification of IHC staining (% area stained) was performed on each of the digitized slides using Biospective's PERMITS process. Additionally, co-localization of pTDP-43 and NeuN was calculated from the segmented images. The IF analysis and quantification were performed in a blind manner with respect to cohort. The data shown in Figures 6, S12, S13, S14, and S15 represent individual animals, with quantification based on one coronal brain section per animal. For each section, the entire region of interest (e.g., hippocampus and cortex) was used for analysis.

DATA AND CODE AVAILABILITY

The data that support the findings of this study are available from the corresponding author, D.N., upon reasonable request.

ACKNOWLEDGMENTS

We would like to thank Prof. Virginia Lee and Dr. Silvia Porta for providing an expert opinion in the setting up of the mouse model. We thank Elodie Brison, Kristina Deduck, and Barry Bedell from Biospective (Canada) for providing insight on mouse models and performing the *in vivo* experiments presented in this study. We thank Madiha Derouazi, Mateusz Kozak, Aline Fuchs, Davide Basco, Florian Udry, Paula Stephen, and Bojana Portmann for their constructive feedback on the experiment designs and manuscript. We thank Prof. William Seeley and Neurodegenerative Disease Brain Bank UCSF (funding support from NIH grants P01AG019724 and P50AG023501, the Consortium for Frontotemporal Dementia Research, and the Tau Consortium); Netherlands Institute for Neuroscience, Amsterdam; Prof. Tammaryn Lashley; and Queen Square Brain Bank for Neurological Disorders, UCL. The graphical abstract and some figures were created using BioRender (Nevoltris, D. [2025] https://BioRender.com/b42s541).

This study was funded by AC Immune SA.

Informed consent for autopsy and usage of tissue for research purposes had been obtained from probands or their legal representative in accordance with local institutional review boards. All animal procedures were performed according to institutional guidelines approved by respective country's governmental ethics committee.

AUTHOR CONTRIBUTIONS

M.K.-V., A.P., G.d.V., and D.N. conceived the study. G.d.V., F.G., M.A., S.M., M.R., E.C., R.O., D.B., T.S., and T.A. contributed to the experiments in design, execution, and interpretation. G.d.V., M.K.-V., and D.N. wrote the manuscript.

DECLARATION OF INTERESTS

D.N. and. G.d.V. are coinventors on a patent application, publication number WO2022/129609. G.d.V., F.G., S.M., E.C., R.O., T.S., A.P., M.K.-V., and D.N. are employees of AC Immune and are entitled to options and/or shares. M.A., D.B., M.R., and T.A. were employees of AC Immune at the time of this study.

This study was funded by AC Immune SA.

SUPPLEMENTAL INFORMATION

Supplemental information can be found online at https://doi.org/10.1016/j.ymthe.2025. 06.026.

REFERENCES

- Prasad, A., Bharathi, V., Sivalingam, V., Girdhar, A., and Patel, B.K. (2019).
 Molecular Mechanisms of TDP-43 Misfolding and Pathology in Amyotrophic Lateral Sclerosis. Front. Mol. Neurosci. 12, 25. https://doi.org/10.3389/fnmol.2019.
- 2. Neumann, M., Sampathu, D.M., Kwong, L.K., Truax, A.C., Micsenyi, M.C., Chou, T. T., Bruce, J., Schuck, T., Grossman, M., Clark, C.M., et al. (2006). Ubiquitinated

- TDP-43 in frontotemporal lobar degeneration and amyotrophic lateral sclerosis. Science 314, 130–133. https://doi.org/10.1126/science.1134108.
- Liao, Y.Z., Ma, J., and Dou, J.Z. (2022). The Role of TDP-43 in Neurodegenerative Disease. Mol. Neurobiol. 59, 4223–4241. https://doi.org/10.1007/s12035-022-02847-x.
- Shao, W., Todd, T.W., Wu, Y., Jones, C.Y., Tong, J., Jansen-West, K., Daughrity, L. M., Park, J., Koike, Y., Kurti, A., et al. (2022). Two FTD-ALS genes converge on the endosomal pathway to induce TDP-43 pathology and degeneration. Science 378, 94–99. https://doi.org/10.1126/science.abq7860.
- Nelson, P.T., Dickson, D.W., Trojanowski, J.Q., Jack, C.R., Boyle, P.A., Arfanakis, K., Rademakers, R., Alafuzoff, I., Attems, J., Brayne, C., et al. (2019). Limbic-predominant age-related TDP-43 encephalopathy (LATE): consensus working group report. Brain 142, 1503–1527. https://doi.org/10.1093/brain/awz099.
- Tan, R.H., Ke, Y.D., Ittner, L.M., and Halliday, G.M. (2017). ALS/FTLD: experimental models and reality. Acta Neuropathol. 133, 177–196. https://doi.org/10.1007/s00401-016-1666-6.
- Mackenzie, I.R., Rademakers, R., and Neumann, M. (2010). TDP-43 and FUS in amyotrophic lateral sclerosis and frontotemporal dementia. Lancet Neurol. 9, 995–1007. https://doi.org/10.1016/s1474-4422(10)70195-2.
- Meneses, A., Koga, S., O'Leary, J., Dickson, D.W., Bu, G., and Zhao, N. (2021). TDP-43 Pathology in Alzheimer's Disease. Mol. Neurodegener. 16, 84. https://doi.org/10.1186/s13024-021-00503-x.
- Cook, C., Zhang, Y.J., Xu, Y.F., Dickson, D.W., and Petrucelli, L. (2008). TDP-43 in neurodegenerative disorders. Expert Opin. Biol. Ther. 8, 969–978. https://doi.org/ 10.1517/14712598.8.7.969.
- Jo, M., Lee, S., Jeon, Y.M., Kim, S., Kwon, Y., and Kim, H.J. (2020). The role of TDP-43 propagation in neurodegenerative diseases: integrating insights from clinical and experimental studies. Exp. Mol. Med. 52, 1652–1662. https://doi.org/10.1038/ s12276-020-00513-7.
- Hergesheimer, R.C., Chami, A.A., de Assis, D.R., Vourc'h, P., Andres, C.R., Corcia, P., Lanznaster, D., and Blasco, H. (2019). The debated toxic role of aggregated TDP-43 in amyotrophic lateral sclerosis: a resolution in sight? Brain 142, 1176–1194. https://doi.org/10.1093/brain/awz078.
- Tzeplaeff, L., Wilfling, S., Requardt, M.V., and Herdick, M. (2023). Current State and Future Directions in the Therapy of ALS. Cells 12, 1523. https://doi.org/10.3390/ cells12111523
- Wiesenfarth, M., Dorst, J., Brenner, D., Elmas, Z., Parlak, Ö., Uzelac, Z., Kandler, K., Mayer, K., Weiland, U., Herrmann, C., et al. (2024). Effects of tofersen treatment in patients with SOD1-ALS in a "real-world" setting - a 12-month multicenter cohort study from the German early access program. EClinicalMedicine 69, 102495. https:// doi.org/10.1016/j.eclinm.2024.102495.
- Afroz, T., Chevalier, E., Audrain, M., Dumayne, C., Ziehm, T., Moser, R., Egesipe, A. L., Mottier, L., Ratnam, M., Neumann, M., et al. (2023). Immunotherapy targeting the C-terminal domain of TDP-43 decreases neuropathology and confers neuroprotection in mouse models of ALS/FTD. Neurobiol. Dis. 179, 106050. https://doi.org/ 10.1016/j.nbd.2023.106050.
- Li, C., and Samulski, R.J. (2020). Engineering adeno-associated virus vectors for gene therapy. Nat. Rev. Genet. 21, 255–272. https://doi.org/10.1038/s41576-019-0205-4.
- Chng, J., Wang, T., Nian, R., Lau, A., Hoi, K.M., Ho, S.C.L., Gagnon, P., Bi, X., and Yang, Y. (2015). Cleavage efficient 2A peptides for high level monoclonal antibody expression in CHO cells. MAbs 7, 403–412. https://doi.org/10.1080/19420862.2015. 1008351.
- Mizote, Y., Masumi-Koizumi, K., Katsuda, T., and Yamaji, H. (2020). Production of an antibody Fab fragment using 2A peptide in insect cells. J. Biosci. Bioeng. 130, 205–211. https://doi.org/10.1016/j.jbiosc.2020.03.009.
- Fuchs, S.P., and Desrosiers, R.C. (2016). Promise and problems associated with the use of recombinant AAV for the delivery of anti-HIV antibodies. Mol. Ther. Methods Clin. Dev. 3, 16068. https://doi.org/10.1038/mtm.2016.68.
- Ho, S.C.L., Koh, E.Y.C., van Beers, M., Mueller, M., Wan, C., Teo, G., Song, Z., Tong, Y.W., Bardor, M., and Yang, Y. (2013). Control of IgG LC:HC ratio in stably transfected CHO cells and study of the impact on expression, aggregation, glycosylation and conformational stability. J. Biotechnol. 165, 157–166. https://doi.org/10.1016/j. jbiotec.2013.03.019.

- Yeo, J.H.M., Mariati, and Yang, Y. (2018). An IRES-Mediated Tricistronic Vector for Efficient Generation of Stable, High-Level Monoclonal Antibody Producing CHO DG44 Cell Lines. Methods Mol. Biol. 1827, 335–349. https://doi.org/10.1007/978-1-4939-8648-4_17.
- Schneider, K.T., Kirmann, T., Wenzel, E.V., Grosch, J.H., Polten, S., Meier, D., Becker, M., Matejtschuk, P., Hust, M., Russo, G., and Dübel, S. (2021). Shelf-Life Extension of Fc-Fused Single Chain Fragment Variable Antibodies by Lyophilization. Front. Cell. Infect. Microbiol. 11, 717689. https://doi.org/10.3389/ fcimb.2021.717689.
- Pipe, S., Leebeek, F.W.G., Ferreira, V., Sawyer, E.K., and Pasi, J. (2019). Clinical Considerations for Capsid Choice in the Development of Liver-Targeted AAV-Based Gene Transfer. Mol. Ther. Methods Clin. Dev. 15, 170–178. https://doi.org/ 10.1016/j.omtm.2019.08.015.
- Hammond, S.L., Leek, A.N., Richman, E.H., and Tjalkens, R.B. (2017). Cellular selectivity of AAV serotypes for gene delivery in neurons and astrocytes by neonatal intracerebroventricular injection. PLoS One 12, e0188830. https://doi.org/10.1371/ journal.pone.0188830.
- Sorrentino, N.C., Maffia, V., Strollo, S., Cacace, V., Romagnoli, N., Manfredi, A., Ventrella, D., Dondi, F., Barone, F., Giunti, M., et al. (2016). A Comprehensive Map of CNS Transduction by Eight Recombinant Adeno-associated Virus Serotypes Upon Cerebrospinal Fluid Administration in Pigs. Mol. Ther. 24, 276–286. https://doi.org/10.1038/mt.2015.212.
- Lisowski, L., Tay, S.S., and Alexander, I.E. (2015). Adeno-associated virus serotypes for gene therapeutics. Curr. Opin. Pharmacol. 24, 59–67. https://doi.org/10.1016/j. coph.2015.07.006.
- Korbelin, J., Dogbevia, G., Michelfelder, S., Ridder, D.A., Hunger, A., Wenzel, J., Seismann, H., Lampe, M., Bannach, J., Pasparakis, M., et al. (2016). A brain microvasculature endothelial cell-specific viral vector with the potential to treat neurovascular and neurological diseases. EMBO Mol. Med. 8, 609–625. https://doi.org/10. 15252/emmm.201506078.
- 27. Weber-Adrian, D., Heinen, S., Silburt, J., Noroozian, Z., and Aubert, I. (2017). The human brain endothelial barrier: transcytosis of AAV9, transduction by AAV2: An Editorial Highlight for "Trafficking of adeno-associated virus vectors across a model of the blood-brain barrier; a comparative study of transcytosis and transduction using primary human brain endothelial cells. J. Neurochem. 140, 192–194. https://doi.org/10.1111/jinc.13898.
- Jones, E.V., and Bouvier, D.S. (2014). Astrocyte-secreted matricellular proteins in CNS remodelling during development and disease. Neural Plast. 2014, 321209. https://doi.org/10.1155/2014/321209.
- Kügler, S., Kilic, E., and Bähr, M. (2003). Human synapsin 1 gene promoter confers highly neuron-specific long-term transgene expression from an adenoviral vector in the adult rat brain depending on the transduced area. Gene Ther. 10, 337–347. https://doi.org/10.1038/sj.gt.3301905.
- Shevtsova, Z., Malik, J.M.I., Michel, U., Bähr, M., and Kügler, S. (2005). Promoters and serotypes: targeting of adeno-associated virus vectors for gene transfer in the rat central nervous system in vitro and in vivo. Exp. Physiol. 90, 53–59. https://doi.org/ 10.1113/expphysiol.2004.028159.
- 31. Gray, S.J., Foti, S.B., Schwartz, J.W., Bachaboina, L., Taylor-Blake, B., Coleman, J., Ehlers, M.D., Zylka, M.J., McCown, T.J., and Samulski, R.J. (2011). Optimizing promoters for recombinant adeno-associated virus-mediated gene expression in the peripheral and central nervous system using self-complementary vectors. Hum. Gene Ther. 22, 1143–1153. https://doi.org/10.1089/hum.2010.245.
- Dreos, R., Ambrosini, G., Périer, R.C., and Bucher, P. (2015). The Eukaryotic Promoter Database: expansion of EPDnew and new promoter analysis tools. Nucleic Acids Res. 43, D92–D96. https://doi.org/10.1093/nar/gku1111.
- Meylan, P., Dreos, R., Ambrosini, G., Groux, R., and Bucher, P. (2020). EPD in 2020: enhanced data visualization and extension to ncRNA promoters. Nucleic Acids Res. 48, D65–D69. https://doi.org/10.1093/nar/gkz1014.
- Chuecos, M.A., and Lagor, W.R. (2024). Liver directed adeno-associated viral vectors to treat metabolic disease. J. Inherit. Metab. Dis. 47, 22–40. https://doi.org/10.1002/jimd.12637.
- Davidoff, A.M., Ng, C.Y.C., Zhou, J., Spence, Y., and Nathwani, A.C. (2003). Sex significantly influences transduction of murine liver by recombinant adeno-associ-

- ated viral vectors through an androgen-dependent pathway. Blood 102, 480–488. https://doi.org/10.1182/blood-2002-09-2889.
- Berraondo, P., Crettaz, J., Ochoa, L., Pañeda, A., Prieto, J., Trocóniz, I.F., and González-Aseguinolaza, G. (2006). Intrahepatic injection of recombinant adenoassociated virus serotype 2 overcomes gender-related differences in liver transduction. Hum. Gene Ther. 17, 601–610. https://doi.org/10.1089/hum.2006.17.601.
- 37. Pañeda, A., Vanrell, L., Mauleon, I., Crettaz, J.S., Berraondo, P., Timmermans, E.J., Beattie, S.G., Twisk, J., van Deventer, S., Prieto, J., et al. (2009). Effect of adeno-associated virus serotype and genomic structure on liver transduction and biodistribution in mice of both genders. Hum. Gene Ther. 20, 908–917. https://doi.org/10.1089/hum.2009.031.
- 38. van den Berg, F.T., Makoah, N.A., Ali, S.A., Scott, T.A., Mapengo, R.E., Mutsvunguma, L.Z., Mkhize, N.N., Lambson, B.E., Kgagudi, P.D., Crowther, C., et al. (2019). AAV-Mediated Expression of Broadly Neutralizing and Vaccine-like Antibodies Targeting the HIV-1 Envelope V2 Region. Mol. Ther. Methods Clin. Dev. 14, 100–112. https://doi.org/10.1016/j.omtm.2019.06.002.
- Kadry, H., Noorani, B., and Cucullo, L. (2020). A blood-brain barrier overview on structure, function, impairment, and biomarkers of integrity. Fluids Barriers CNS 17, 69. https://doi.org/10.1186/s12987-020-00230-3.
- Terstappen, G.C., Meyer, A.H., Bell, R.D., and Zhang, W. (2021). Strategies for delivering therapeutics across the blood-brain barrier. Nat. Rev. Drug Discov. 20, 362–383. https://doi.org/10.1038/s41573-021-00139-y.
- Porta, S., Xu, Y., Restrepo, C.R., Kwong, L.K., Zhang, B., Brown, H.J., Lee, E.B., Trojanowski, J.Q., and Lee, V.M.Y. (2018). Patient-derived frontotemporal lobar degeneration brain extracts induce formation and spreading of TDP-43 pathology in vivo. Nat. Commun. 9, 4220. https://doi.org/10.1038/s41467-018-06548-9.
- Marchi, P.M., Marrone, L., and Azzouz, M. (2022). Delivery of therapeutic AAV9 vectors via cisterna magna to treat neurological disorders. Trends Mol. Med. 28, 79–80. https://doi.org/10.1016/j.molmed.2021.09.007.
- Sevigny, J., Uspenskaya, O., Heckman, L.D., Wong, L.C., Hatch, D.A., Tewari, A., Vandenberghe, R., Irwin, D.J., Saracino, D., Le Ber, I., et al. (2024). Progranulin AAV gene therapy for frontotemporal dementia: translational studies and phase 1/2 trial interim results. Nat. Med. 30, 1406–1415. https://doi.org/10.1038/s41591-024-02973-0
- 44. Igaz, L.M., Kwong, L.K., Lee, E.B., Chen-Plotkin, A., Swanson, E., Unger, T., Malunda, J., Xu, Y., Winton, M.J., Trojanowski, J.Q., and Lee, V.M.Y. (2011). Dysregulation of the ALS-associated gene TDP-43 leads to neuronal death and degeneration in mice. J. Clin. Invest. 121, 726–738. https://doi.org/10.1172/jci44867.
- Chevalier, E., Audrain, M., Ratnam, M., Ollier, R., Fuchs, A., Piorkowska, K., Pfeifer, A., Kosco-Vilbois, M., Seredenina, T., and Afroz, T. (2024). Targeting the TDP-43 low complexity domain blocks spreading of pathology in a mouse model of ALS/ FTD. Acta Neuropathol. Commun. 12, 156. https://doi.org/10.1186/s40478-024-01867-z.
- Gross, D.A., Tedesco, N., Leborgne, C., and Ronzitti, G. (2022). Overcoming the Challenges Imposed by Humoral Immunity to AAV Vectors to Achieve Safe and Efficient Gene Transfer in Seropositive Patients. Front. Immunol. 13, 857276. https://doi.org/10.3389/fimmu.2022.857276.
- Earley, J., Piletska, E., Ronzitti, G., and Piletsky, S. (2023). Evading and overcoming AAV neutralization in gene therapy. Trends Biotechnol. 41, 836–845. https://doi. org/10.1016/j.tibtech.2022.11.006.
- Dhungel, B.P., Winburn, I., Pereira, C.D.F., Huang, K., Chhabra, A., and Rasko, J.E.J. (2024). Understanding AAV vector immunogenicity: from particle to patient. Theranostics 14, 1260–1288. https://doi.org/10.7150/thno.89380.
- Fuchs, S.P., Martinez-Navio, J.M., Gao, G., and Desrosiers, R.C. (2016).
 Recombinant AAV Vectors for Enhanced Expression of Authentic IgG. PLoS One 11, e0158009. https://doi.org/10.1371/journal.pone.0158009.
- Wu, D., Hwang, P., Li, T., and Piszczek, G. (2022). Rapid characterization of adenoassociated virus (AAV) gene therapy vectors by mass photometry. Gene Ther. 29, 691–697. https://doi.org/10.1038/s41434-021-00311-4.
- Fukuchi, K.i., Tahara, K., Kim, H.D., Maxwell, J.A., Lewis, T.L., Accavitti-Loper, M. A., Kim, H., Ponnazhagan, S., and Lalonde, R. (2006). Anti-Abeta single-chain anti-body delivery via adeno-associated virus for treatment of Alzheimer's disease. Neurobiol. Dis. 23, 502–511. https://doi.org/10.1016/j.nbd.2006.04.012.

- Pozzi, S., Thammisetty, S.S., Codron, P., Rahimian, R., Plourde, K.V., Soucy, G., Bareil, C., Phaneuf, D., Kriz, J., Gravel, C., and Julien, J.P. (2019). Virus-mediated delivery of antibody targeting TAR DNA-binding protein-43 mitigates associated neuropathology. J. Clin. Invest. 129, 1581–1595. https://doi.org/10.1172/JCI123931.
- 53. Elmer, B.M., Swanson, K.A., Bangari, D.S., Piepenhagen, P.A., Roberts, E., Taksir, T., Guo, L., Obinu, M.C., Barneoud, P., Ryan, S., et al. (2019). Gene delivery of a modified antibody to Abeta reduces progression of murine Alzheimer's disease. PLoS One 14, e0226245. https://doi.org/10.1371/journal.pone.0226245.
- 54. Hay, C.E., Ewing, L.E., Hambuchen, M.D., Zintner, S.M., Small, J.C., Bolden, C.T., Fantegrossi, W.E., Margaritis, P., Owens, S.M., and Peterson, E.C. (2019). The development and characterization of an scFv-Fc fusion based gene therapy to reduce the psychostimulant effects of methamphetamine abuse. J. Pharmacol. Exp. Ther. 374, 16–23. https://doi.org/10.1101/687129.
- Johnson, P.R., Schnepp, B.C., Zhang, J., Connell, M.J., Greene, S.M., Yuste, E., Desrosiers, R.C., and Clark, K.R. (2009). Vector-mediated gene transfer engenders long-lived neutralizing activity and protection against SIV infection in monkeys. Nat. Med. 15, 901–906. https://doi.org/10.1038/nm.1967.
- Fuchs, S.P., Martinez-Navio, J.M., Piatak, M., Jr., Lifson, J.D., Gao, G., and Desrosiers, R.C. (2015). AAV-Delivered Antibody Mediates Significant Protective Effects against SIVmac239 Challenge in the Absence of Neutralizing Activity. PLoS Pathog. 11, e1005090. https://doi.org/10.1371/journal.ppat.1005090.
- Martinez-Navio, J.M., Fuchs, S.P., Mendes, D.E., Rakasz, E.G., Gao, G., Lifson, J.D., and Desrosiers, R.C. (2020). Long-Term Delivery of an Anti-SIV Monoclonal Antibody With AAV. Front. Immunol. 11, 449. https://doi.org/10.3389/fimmu. 2020.00449.
- Martinez-Navio, J.M., Fuchs, S.P., Pantry, S.N., Lauer, W.A., Duggan, N.N., Keele, B. F., Rakasz, E.G., Gao, G., Lifson, J.D., and Desrosiers, R.C. (2019). Adeno-Associated Virus Delivery of Anti-HIV Monoclonal Antibodies Can Drive Long-Term Virologic Suppression. Immunity 50, 567–575.e5. https://doi.org/10.1016/j.immuni.2019.02.005.
- Marino, M., Zhou, L., Rincon, M.Y., Callaerts-Vegh, Z., Verhaert, J., Wahis, J., Creemers, E., Yshii, L., Wierda, K., Saito, T., et al. (2022). AAV-mediated delivery of an anti-BACE1 VHH alleviates pathology in an Alzheimer's disease model. EMBO Mol. Med. 14, e09824. https://doi.org/10.15252/emmm.201809824.
- Marino, M., and Holt, M.G. (2022). AAV Vector-Mediated Antibody Delivery (A-MAD) in the Central Nervous System. Front. Neurol. 13, 870799. https://doi.org/10.3389/fneur.2022.870799.
- Soetens, E., Ballegeer, M., and Saelens, X. (2020). An Inside Job: Applications of Intracellular Single Domain Antibodies. Biomolecules 10, 1663. https://doi.org/10. 3390/biom10121663.
- 62. Fukuda, N., Noi, K., Weng, L., Kobashigawa, Y., Miyazaki, H., Wakeyama, Y., Takaki, M., Nakahara, Y., Tatsuno, Y., Uchida-Kamekura, M., et al. (2017). Production of Single-Chain Fv Antibodies Specific for GA-Pyridine, an Advanced Glycation End-Product (AGE), with Reduced Inter-Domain Motion. Molecules 22, 1695. https://doi.org/10.3390/molecules22101695.
- Teerinen, T., Valjakka, J., Rouvinen, J., and Takkinen, K. (2006). Structure-based Stability Engineering of the Mouse IgG1 Fab Fragment by Modifying Constant Domains. J. Mol. Biol. 361, 687–697. https://doi.org/10.1016/j.jmb.2006.06.073.
- Quintero-Hernández, V., Juárez-González, V.R., Ortíz-León, M., Sánchez, R., Possani, L.D., and Becerril, B. (2007). The change of the scFv into the Fab format improves the stability and in vivo toxin neutralization capacity of recombinant antibodies. Mol. Immunol. 44, 1307–1315. https://doi.org/10.1016/j.molimm.2006. 05.009.
- Lu, L.L., Suscovich, T.J., Fortune, S.M., and Alter, G. (2018). Beyond binding: antibody effector functions in infectious diseases. Nat. Rev. Immunol. 18, 46–61. https:// doi.org/10.1038/nri.2017.106.
- Thomas, G. (2002). Furin at the cutting edge: from protein traffic to embryogenesis and disease. Nat. Rev. Mol. Cell Biol. 3, 753–766. https://doi.org/10.1038/nrm934.
- Liu, Z., Chen, O., Wall, J.B.J., Zheng, M., Zhou, Y., Wang, L., Vaseghi, H.R., Qian, L., and Liu, J. (2017). Systematic comparison of 2A peptides for cloning multi-genes in a polycistronic vector. Sci. Rep. 7, 2193. https://doi.org/10.1038/s41598-017-02460-2.
- 68. Yang, S., Cohen, C.J., Peng, P.D., Zhao, Y., Cassard, L., Yu, Z., Zheng, Z., Jones, S., Restifo, N.P., Rosenberg, S.A., and Morgan, R.A. (2008). Development of optimal bi-

- cistronic lentiviral vectors facilitates high-level TCR gene expression and robust tumor cell recognition. Gene Ther. 15, 1411–1423. https://doi.org/10.1038/gt.2008.90.
- Sharma, P., Yan, F., Doronina, V.A., Escuin-Ordinas, H., Ryan, M.D., and Brown, J. D. (2012). 2A peptides provide distinct solutions to driving stop-carry on translational recoding. Nucleic Acids Res. 40, 3143–3151. https://doi.org/10.1093/nar/gkt1176
- Kim, J.H., Lee, S.R., Li, L.H., Park, H.J., Park, J.H., Lee, K.Y., Kim, M.K., Shin, B.A., and Choi, S.Y. (2011). High cleavage efficiency of a 2A peptide derived from porcine teschovirus-1 in human cell lines, zebrafish and mice. PLoS One 6, e18556. https:// doi.org/10.1371/journal.pone.0018556.
- Velychko, S., Kang, K., Kim, S.M., Kwak, T.H., Kim, K.P., Park, C., Hong, K., Chung, C., Hyun, J.K., MacCarthy, C.M., et al. (2019). Fusion of Reprogramming Factors Alters the Trajectory of Somatic Lineage Conversion. Cell Rep. 27, 30–39.e4. https://doi.org/10.1016/j.celrep.2019.03.023.
- Saunders, K.O., Wang, L., Joyce, M.G., Yang, Z.Y., Balazs, A.B., Cheng, C., Ko, S.Y., Kong, W.P., Rudicell, R.S., Georgiev, I.S., et al. (2015). Broadly Neutralizing Human Immunodeficiency Virus Type 1 Antibody Gene Transfer Protects Nonhuman Primates from Mucosal Simian-Human Immunodeficiency Virus Infection. J. Virol. 89, 8334–8345. https://doi.org/10.1128/JVI.00908-15.
- Zhu, X., Ricci-Tam, C., Hager, E.R., and Sgro, A.E. (2023). Self-cleaving peptides for expression of multiple genes in Dictyostelium discoideum. PLoS One 18, e0281211. https://doi.org/10.1371/journal.pone.0281211.
- Mizuguchi, H., Xu, Z., Ishii-Watabe, A., Uchida, E., and Hayakawa, T. (2000). IRES-dependent second gene expression is significantly lower than cap-dependent first gene expression in a bicistronic vector. Mol. Ther. 1, 376–382. https://doi.org/10.1006/mthe.2000.0050.
- Ho, S.C.L., Bardor, M., Feng, H., Yang, Y., Mariati, Tong, Y.W., Tong, Y.W., Song, Z., and Yap, M.G.S. (2012). IRES-mediated Tricistronic vectors for enhancing generation of high monoclonal antibody expressing CHO cell lines. J. Biotechnol. 157, 130–139. https://doi.org/10.1016/j.jbiotec.2011.09.023.
- Simon, M.J., and Iliff, J.J. (2016). Regulation of cerebrospinal fluid (CSF) flow in neurodegenerative, neurovascular and neuroinflammatory disease. Biochim. Biophys. Acta 1862, 442–451. https://doi.org/10.1016/j.bbadis.2015.10.014.
- 77. Rosenberg, J.B., Fung, E.K., Dyke, J.P., De, B.P., Lou, H., Kelly, J.M., Reejhsinghani, L., Ricart Arbona, R.J., Sondhi, D., Kaminsky, S.M., et al. (2023). Positron Emission Tomography Quantitative Assessment of Off-Target Whole-Body Biodistribution of I-124-Labeled Adeno-Associated Virus Capsids Administered to Cerebral Spinal Fluid. Hum. Gene Ther. 34, 1095–1106. https://doi.org/10.1089/hum.2023.060.
- Bailey, R.M., Rozenberg, A., and Gray, S.J. (2020). Comparison of high-dose intracisterna magna and lumbar puncture intrathecal delivery of AAV9 in mice to treat neuropathies. Brain Res. 1739, 146832. https://doi.org/10.1016/j.brainres.2020.
- Ballon, D.J., Rosenberg, J.B., Fung, E.K., Nikolopoulou, A., Kothari, P., De, B.P., He, B., Chen, A., Heier, L.A., Sondhi, D., et al. (2020). Quantitative Whole-Body Imaging of I-124-Labeled Adeno-Associated Viral Vector Biodistribution in Nonhuman Primates. Hum. Gene Ther. 31, 1237–1259. https://doi.org/10.1089/hum.2020.116.
- Lukashchuk, V., Lewis, K.E., Coldicott, I., Grierson, A.J., and Azzouz, M. (2016).
 AAV9-mediated central nervous system-targeted gene delivery via cisterna magna route in mice. Mol. Ther. Methods Clin. Dev. 3, 15055. https://doi.org/10.1038/mtm.2015.55.
- Foust, K.D., Nurre, E., Montgomery, C.L., Hernandez, A., Chan, C.M., and Kaspar, B.K. (2009). Intravascular AAV9 preferentially targets neonatal neurons and adult astrocytes. Nat. Biotechnol. 27, 59–65. https://doi.org/10.1038/nbt.1515.
- Okada, Y., Hosoi, N., Matsuzaki, Y., Fukai, Y., Hiraga, A., Nakai, J., Nitta, K., Shinohara, Y., Konno, A., and Hirai, H. (2022). Development of microglia-targeting adeno-associated viral vectors as tools to study microglial behavior in vivo. Commun. Biol. 5, 1224. https://doi.org/10.1038/s42003-022-04200-3.
- Chatterjee, D., Marmion, D.J., McBride, J.L., Manfredsson, F.P., Butler, D., Messer, A., and Kordower, J.H. (2022). Enhanced CNS transduction from AAV.PHP.eB infusion into the cisterna magna of older adult rats compared to AAV9. Gene Ther. 29, 390–397. https://doi.org/10.1038/s41434-021-00244-y.
- 84. Huang, Q., Chan, K.Y., Lou, S., Keyes, C., Wu, J., Botticello-Romero, N.R., Zheng, Q., Johnston, J., Mills, A., Brauer, P.P., et al. (2023). An AAV capsid reprogrammed

- to bind human Transferrin Receptor mediates brain-wide gene delivery. Preprint at bioRxiv. https://doi.org/10.1101/2023.12.20.572615.
- Chuapoco, M.R., Flytzanis, N.C., Goeden, N., Christopher Octeau, J., Roxas, K.M., Chan, K.Y., Scherrer, J., Winchester, J., Blackburn, R.J., Campos, L.J., et al. (2023).
 Adeno-associated viral vectors for functional intravenous gene transfer throughout the non-human primate brain. Nat. Nanotechnol. 18, 1241–1251. https://doi.org/10. 1038/s41565-023-01419-x.
- Wang, J.H., Gessler, D.J., Zhan, W., Gallagher, T.L., and Gao, G. (2024). Adeno-associated virus as a delivery vector for gene therapy of human diseases. Signal Transduct. Target. Ther. 9, 78. https://doi.org/10.1038/s41392-024-01780-w.
- 87. Zecca, C., Dell'Abate, M.T., Capozzo, R., Introna, A., Barone, R., Barulli, M.R., Battista, P., and Logroscino, G. (2020). Cerebrospinal Fluid TDP-43 is a Possible Predictor of Survival in Amyotrophic Lateral Sclerosis (4143). Neurology 94, 4143. https://doi.org/10.1212/WNL.94.15_supplement.4143.
- Kasai, T., Tokuda, T., Ishigami, N., Sasayama, H., Foulds, P., Mitchell, D.J., Mann, D. M.A., Allsop, D., and Nakagawa, M. (2009). Increased TDP-43 protein in cerebrospinal fluid of patients with amyotrophic lateral sclerosis. Acta Neuropathol. 117, 55–62. https://doi.org/10.1007/s00401-008-0456-1.

- Ayuso, E., Mingozzi, F., Montane, J., Leon, X., Anguela, X.M., Haurigot, V., Edmonson, S.A., Africa, L., Zhou, S., High, K.A., et al. (2010). High AAV vector purity results in serotype- and tissue-independent enhancement of transduction efficiency. Gene Ther. 17, 503-510. https://doi.org/10.1038/gt. 2009.157.
- Lee, Y., Messing, A., Su, M., and Brenner, M. (2008). GFAP promoter elements required for region-specific and astrocyte-specific expression. Glia 56, 481–493. https://doi.org/10.1002/glia.20622.
- Boshart, M., Weber, F., Jahn, G., Dorsch-Häsler, K., Fleckenstein, B., and Schaffner, W. (1985). A very strong enhancer is located upstream of an immediate early gene of human cytomegalovirus. Cell 41, 521–530. https://doi.org/10.1016/s0092-8674(85) 80025-8.
- Laferrière, F., Maniecka, Z., Pérez-Berlanga, M., Hruska-Plochan, M., Gilhespy, L., Hock, E.M., Wagner, U., Afroz, T., Boersema, P.J., Barmettler, G., et al. (2019). TDP-43 extracted from frontotemporal lobar degeneration subject brains displays distinct aggregate assemblies and neurotoxic effects reflecting disease progression rates. Nat. Neurosci. 22, 65–77. https://doi.org/10.1038/s41593-018-0294-y.